NASA TECHNICAL NOTE

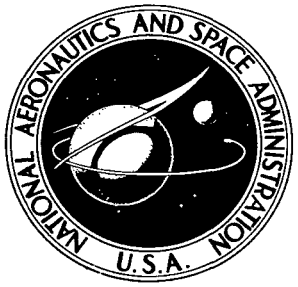

NASA TN D-4742

A CELESTIAL ATTITUDE MEASUREMENT INSTRUMENT FOR PROJECT SCANNER

by T. M. Walsh, William C. Dixon, Jr., Dwayne E. Hinton, and James A. Holland

Langley Research Center
Langley Station, Hampton, Va.

NATIONAL AERONAUTICS AND SPACE ADMINISTRATION • WASHINGTON, D. C. • AUGUST 1968

NASA TN D-4742

A CELESTIAL ATTITUDE MEASUREMENT INSTRUMENT FOR PROJECT SCANNER

By T. M. Walsh, William C. Dixon, Jr., Dwayne E. Hinton, and James A. Holland

Langley Research Center
Langley Station, Hampton, Va.

NATIONAL AERONAUTICS AND SPACE ADMINISTRATION

For sale by the Clearinghouse for Federal Scientific and Technical Information
Springfield, Virginia 22151 – CFSTI price $3.00

A CELESTIAL ATTITUDE MEASUREMENT INSTRUMENT FOR PROJECT SCANNER

By T. M. Walsh, William C. Dixon, Jr., Dwayne E. Hinton, and James A. Holland
Langley Research Center

SUMMARY

The Project Scanner horizon-definition experiment required independent spacecraft attitude measurements with an accuracy (1σ) of 0.016^{o}. This requirement led to the development of a celestial attitude measurement procedure using a unique star-mapping technique. Successful application of this technique required the detection and identification of stars in a +3 visual magnitude A0 spectral class.

Star mapping was accomplished by use of a passive optical instrument consisting of a telescope, a coded reticle, and a photomultiplier. The telescope was mounted with its optical axis normal to the Scanner spacecraft principal spin axis. Spin motion about this axis caused star images to transit the reticle. Each star transit was sensed by the photomultiplier as two sequences of coded pulses that were telemetered to a ground receiving station. The amplitudes of the received pulses were proportional to the photometric magnitude of the stars, and the time separation of two pulse groups generated by a single star transit were related to the elevation angle of the star within the field of view of the telescope. Time separations of pulse groups generated by different stars were related to their azimuth angle separations. Total-angular-separation computations were used to identify the stars.

The design of the star mapper is discussed and a description of the optics, photomultiplier, reticle, electronics, and sun shield is included. A brief discussion of the techniques used for processing the Project Scanner star-mapper signals is also included. Results from Scanner flights 1 and 2 are summarized in the form of listing of stars that were detected and identified during these two flights. These results demonstrated that the design goal of detecting and identifying stars in the +3 visual magnitude A0 spectral class was met.

INTRODUCTION

Langley Research Center has been engaged in a series of experiments designed to obtain flight measurements of the horizon radiance profiles of the earth. The intent of

these experiments is to provide necessary basic information to design and evaluate sensors that utilize the limb or horizon of the earth for spacecraft-attitude measurement purposes. The recently completed Project Scanner horizon-definition experiment used a spin-stabilized spacecraft launched into a suborbital trajectory. The objectives of the experiment were to obtain horizon radiance measurements in the 14-to-16-micron and in the 20-to-35-micron regions of the electromagnetic spectrum (ref. 1). A brief description of the Project Scanner spacecraft is given in table 1.

Determination of the positions of these high-resolution horizon radiance profiles relative to the earth required that the instantaneous spacecraft celestial attitude be determined with an accuracy (1σ) of 0.016° (ref. 2). This requirement led to the development of a unique technique of star mapping for use in attitude determination. A simplified representation of star mapping is illustrated by figure 1. As shown in the figure, spacecraft spin motion scans the field of view of a completely passive optical system about the celestial sphere. Detection and identification of stars falling within the field of view result in a star map that is descriptive of spacecraft attitude relative to the celestial sphere. Instantaneous spacecraft attitude at the time of each star sighting can be determined by correlating the generated star map with known stellar positions.

The design of the star mapper is discussed and a description of the optics, photomultiplier, reticle, electronics, and sun shield is included. A brief discussion of the techniques used for processing the Project Scanner star-mapper signals is also included. Results from Scanner flights 1 and 2 are summarized in the form of listing of stars that were detected and identified during these two flights.

STAR-MAPPER CONCEPT

The basic star-mapper concept is illustrated by figure 2. The star mapper consists of a telescope, a coded reticle, and a photomultiplier tube. The unit is mounted with its optical axis nominally normal to the spin axis of the Project Scanner spacecraft. The reticle is centered in the focal plane of the telescope with the photomultiplier mounted behind the reticle. The reticle is opaque except for two coded sequences of transparent slits grouped in the general shape of a "V." The spinning motion of the vehicle causes a star image to transit the reticle slits; consequently, a series of pulses of radiant energy will be sensed by the photomultiplier for each star transit of the two sequences of transparent slits. Each sequence of transparent slits in the star mapper was designed to generate an 8-bit code group in which the presence of a star was indicated by a one and the absence was indicated by a zero. The elapsed time (Δt_1) between a pair of pulse groups produced by a single star is related to the elevation angle of that star in the field of view of the star mapper. The elapsed time (Δt_2) between pulse groups produced by a pair of stars is related to their azimuth angle separation.

A simplified flow diagram of the Scanner star-mapper signals is shown in figure 3. The output signals of the star mapper were used to frequency-modulate a telemetry transmitter. These telemetry signals were transmitted to a ground station and were tape recorded by using pre-detection techniques. Processing of these recorded signals consisted of four significant operations: time detection of apparent star transit signals, manual sorting of the apparent transit times to reduce false alarms, identification of the detected stars, and determination of the spacecraft attitude time history. The first two operations are discussed in this report and the last two are discussed in reference 2.

The recorded star-mapper signals along with range time were processed by a pulse-code detector that identified the transit times for each detected star signal. A variable threshold control was adjusted to limit the number of detected star signals, and the peak amplitude of the first pulse in the sequence of pulses generated by a star was recorded for purposes of classifying the stars according to their signal levels.

DESIGN CONSIDERATIONS

In order to determine unambiguously the attitude of a spin-stabilized vehicle through use of celestial observations, at least three celestial bodies must be sighted and identified for each revolution of the vehicle. Based on star distributions in the celestial sphere, it has been determined that a minimum detectable star of +3 visual magnitude (m_V) combined with a 6^o by 6^o field of view scanned through 360^o of the celestial sphere will satisfy the three-body-sighting requirement when the density of the stars contained within the scanned field of view approximates the star density of the mean galactic latitude (ref. 3). The launch windows for the Project Scanner flights were selected to insure that the density of stars viewed by the star mapper would approximate the star density of the mean galactic latitude.

Since the basic star-mapper measurement is the time a star image transits a reticle slit, the instrument accuracy is determined by the resolution of time detection of a star pulse. Therefore, in design, it is necessary to consider not only the optical field distortion and reticle inaccuracies but also the optical image quality and electronic system fidelity that affect the star-signal pulse shape. The optical and electronic design requirements are further constrained by the specific flight requirements. On Project Scanner these requirements were a 270-deg/sec spin rate, a day or night operation, a mechanical envelope of 40.64 by 25.40 by 54.61 centimeters, and a mass limitation of 18 kilograms.

The Project Scanner experiment required that the spacecraft attitude be determined continuously with an accuracy (1σ) of 0.016^o. As a means of insuring that the experiment accuracy requirement was met, a 1σ accuracy of 0.006^o was established for sightings of

individual stars. This accuracy of 0.006^{o} included the effects of optical resolution, reticle slit widths, and a 10-microsecond time resolution of range-time measurements.

Ideally, the optical resolution and basic slit width would have been equal to achieve a matched-filter relationship for purposes of detecting the presence of a pulse. Early program uncertainties in star identification pointed out a possible need for star-signal amplitude measurements for magnitude classification. A slit width of 0.015^{o} and an optical resolution of 0.01^{o} were selected as a compromise between matched-filter characteristics and amplitude-measurement requirements. The resolution of range-time measurements was expected to be 10 microseconds or 0.003^{o} when the spacecraft nominal spin rate of 270 deg/sec was considered. The angular error in sighting an individual star can be estimated by computing the root sum square of the error due to range-time resolution and the error due to the convolution of the optical resolution with the basic slit width. The result of this computation was a 1σ accuracy of approximately 0.006^{o}.

The star signals generated by the photomultiplier are dependent upon the spectral radiant intensity of the star source and the spectral characteristics of the optics and photomultiplier. The spectral radiant intensities of star sources were determined by using source-temperature estimates and assuming blackbody spectra for +3 visual magnitude and brighter stars. A study was performed to determine representative source temperatures for the visual magnitude of interest. The results of this study indicated that the majority of stars of +3 visual magnitude and brighter have source temperatures of 6000^{o} K and hotter (refs. 4 and 5). In addition, the "average" source temperature of the myriad of stars which make up the sky background is 6000^{o} K or colder (refs. 4 and 6). The representative source temperatures clearly indicated that the peak spectral response of the star mapper had to lie toward the short-wavelength region relative to the visual spectrum. Under the consideration of available glass for the optical system and photomultipliers, the short-wavelength cut-off of the instrument was selected to be 3200 angstroms as a design goal. The long-wavelength cut-off of the instrument was selected to be 6000 angstroms to provide a sufficient amount of star irradiance integration for star-signal detection and to reduce the response of the instrument to background light.

The design of a star-mapper unit followed a series of trade-offs between optical transmission, detector sensitivity, optical distortion, reticle design or curvature, background noise, electronic bandwidth, detector dark-current noise, vehicle spin rate, resolution requirements, size, and weight (mass). In the following sections, the star-mapper design is presented along with the more significant trade-offs.

Photodetector

A ruggedized photomultiplier tube having an approximate S-11 spectral response was selected as the photodetector. This tube had a dark current of 1.5×10^{-15} ampere,

had a responsivity of 65 microamperes per lumen, and used 14 dynodes to develop a gain of 10^6 at a nominal supply voltage of 2800 volts dc. The gain stability characteristics of the tube introduced a stringent stray-light requirement, since, when placed in a system capable of detecting a +3 visual magnitude star, a -3 visual magnitude star would cause the tube to exhibit gain degradation; and the tube was virtually destroyed by exposure to light levels brighter than -5 visual magnitude.

Optics

In design of the optics, both reflective and refractive systems were investigated. With a reflective system, it was not possible to take advantage of the space available to provide an effective sun shield. Catadioptric systems were rejected because of the large central obscuration resulting from the secondary mirror.

The refractive optical system chosen for the Project Scanner star mapper was a modified Petzval design with a 38.1-centimeter focal length and a 12.7-centimeter clear aperture. The lens layout, as shown in figure 4, consisted of a cemented doublet, a large lens with an aperture stop located midway through the lens, a second cemented doublet, and a field flattener just in front of the reticle. Behind the reticle were two field lenses which spread the light to cover 75 percent of the photomultiplier cathode surface.

This design provided a maximum blur circle of 0.01° over the field of view. Since it was not possible to obtain a distortion-free image plane, the slits on the reticle were curved slightly to adjust for this problem. The measured spectral response of the entire system (optics and photomultiplier) for the flight 1 star mapper is shown in figure 5.

Reticle

The basic slit width of the reticle is a function of the desired resolution and in the Project Scanner star mapper was made to be 0.015°. The reticle design of the star mapper can be seen in figure 6. By observing the group of vertical slits in the figure (from right- to left-hand side), it can be seen that the first vertical slit was 0.03° wide with a blank width of 0.015° being next, the second vertical slit was 0.015° wide with a blank width of 0.045° being next, and the third vertical slit was 0.015° wide. This grouping provided an 8-bit recognition code of 1-1-0-1-0-0-0-1. The curvature of the vertical slits, required for correction of optical distortion, was approximated by three straight-line segments. No curvature was necessary for the slanted slits since they passed close to the optical axis. The group of slanted slits had an identical recognition code with the narrowest separation between the vertical and slanted code groups being equal to one code group. The choice of the 8-bit code pattern was made to provide a high probability of discriminating stars of +3 visual magnitude and brighter against the expected background (refs. 2 and 3).

Electronics

The output of the photomultiplier tube was amplified by a bandpass amplifier to obtain the desired gain and pulse fidelity. The low-frequency cut-off was required because of slowly varying levels of spatial background noise. The high-frequency cut-off was a function of time of star passage over the narrowest reticle slit, optical resolution (blur circle), and telemetry system filtering. After allowing for spin-rate variation and frequency degradation by signal processing equipment, the high-frequency response was selected to be a three-pole approximation of a Gaussian filter with a -3-decibel point at 33 kilohertz. The low-frequency response was designed to be -3 decibels at 15 hertz with a slope of 6 decibels per octave.

The Project Scanner telemetry system required that the maximum output of the star mapper be 5 volts. To insure that this maximum output of 5 volts was not exceeded, a dynamic range of 0.256 to 4.0 volts was established for +3 to 0 visual magnitude stars of the A0 spectral class (11 000^{o} K), respectively. This dynamic range required a bandpass amplifier gain of approximately 185. A variable gain setting was designed so that amplifier matching to each photomultiplier was possible. The photomultiplier power supply was a solid-state dc-dc converter (28 to 2800 volts). The high voltage level was adjustable over the range of 2300 to 3600 volts dc and was set for each photomultiplier to obtain a gain of 10^{6}. The electrical components (high-voltage power supply, photomultiplier, and bandpass amplifier) were interdependent and required calibration as a unit.

Sun Shield

In order to assure recognition of a +3 visual magnitude A0 star, it was required that the signal levels produced by stray light be less than or equal to the signal level produced by a +4 visual magnitude A0 star. For sunlight, this specification required an attenuation factor of 10^{-12} for all rays entering at angles of 25^{o} or greater from the optical axis. The 25^{o} sun angle was predicated upon the condition that the Scanner launch could be scheduled so that the minimum sun angle was 25^{o} off the optical axis. As shown in figure 7, the star-mapper design did not provide shielding of the optical elements from stray light within a half-cone angle of 19^{o}45'. The sun shield was designed so that all baffle elements were outside the aperture defined by the aperture stop. Consequently, the detector was not able to "see" the sun shield. Furthermore, the baffles were all knife edged, with a 60^{o} bevel, and were spaced 1.27 centimeters apart over the length of the sun shield. All baffles were coated with a high-quality, black, light-absorbent paint. The sun-shield performance was experimentally evaluated and is discussed in a subsequent section.

Instrument Configuration

The final design layout of the star mapper is shown in figure 8. As indicated in this figure, it was necessary to use folding mirrors to meet the Scanner vehicle space limitation. With the addition of these folding mirrors, the overall optical efficiency, including all elements, was approximately 60 percent. An in-flight calibration lamp was installed so that a one-point calibration check could be made periodically throughout the flight to evaluate the system gain stability. A photograph of the assembled star-mapper flight unit is shown in figure 9.

CALIBRATION AND TESTING

Table 2 lists the environmental levels to which the Scanner star mapper was subjected to prove qualification for rocket flight. Operational tests were performed before, during, and after environmental stresses. Optical and alinement degradations were evaluated after each environmental test. Several system tests were performed in addition to the standard operational tests to insure design conformance to specifications. Of particular interest are three of the calibration tests: field-of-view mapping accuracy, photometric calibration, and sun-shield attenuation.

Field-of-View Mapping Accuracy

One of the calibration tests was designed to determine the effects of optical inaccuracies on angular position measurements in the field of view. The basic method employed to determine these inaccuracies was a reconstruction of the reticle through star-mapper measurements and comparison of this reconstructed reticle with the reticle design. The star mapper was rotated so that its field of view scanned a collimated source. The output and the azimuthal angular position of the star mapper were simultaneously recorded. During the scanning process, the image traversed the openings in the reticle. The output signal represented the convolution of the blur circle with the reticle slits. The reticle was reconstructed by plotting the amplitude of the convolved signal against measured azimuth and elevation angles of the star mapper.

Figure 10 is a diagram of the test setup for measuring the field-of-view mapping accuracy. The collimator used for this test has a 254-centimeter focal length and a 25.4-centimeter-diameter primary mirror. The light source was a star simulator, which is discussed in a subsequent section. Measurements were made with an A0 (11 000° K) star and then repeated with a G0 (6000° K) star to examine any possible color effects. The source was chopped at 600 hertz so that a slowly rotating table could be used and still stay in the star-mapper frequency bandwidth. The star mapper was mounted on a 92-centimeter-diameter rotary table with provisions made for varying the elevation angle

of the star mapper relative to the collimated beam by use of sine bars. An optical encoder, with a basic resolution of 2 arc-seconds, was fabricated and fitted to the rotary table to measure azimuth angle as the star mapper scanned the collimated light beam. The small square hole located in the center of the reticle (fig. 6) was used to define 0^{o} azimuth and 0^{o} elevation. The star mapper was leveled and positioned until the star image was at the center of this hole. The angular position of the star mapper was measured by autocollimating off a reference flat mirror placed on the star mapper for this purpose. This measurement defined 0^{o} elevation, and each elevation setting was checked back to this reading. The elevation angle of the star mapper was varied from -2.9^{o} to 2.9^{o} in seven steps. At each elevation setting, the rotary table scanned the field of view of the star mapper through the collimated beam. The table azimuth position and the star-mapper output were recorded at each elevation setting. A plot was made of the output of the star mapper, the elevation setting being the abscissa and the table azimuth position being the ordinate. This plot was compared with the theoretical reticle and was found to agree within 0.01^{o} at all points. An outline of the reticle reconstructed by this method is shown in figure 11.

Photometric Calibration

The ideal means of calibration for a photometric device of this type would be exposure to several stars of different visual magnitudes and spectral classes. However, present knowledge of atmospheric attenuation at any particular time and the presence of scintillation make this method questionable. Therefore, a star simulator was constructed to calibrate the Scanner star mapper.

Star-simulator photometric calibration.- The spectral output of the star simulator was measured by use of a grating monochromator. A quartz-iodine lamp, used as a reference source, was the standard of spectral irradiance. The test setup used for this calibration is shown in figure 12. With the standard of spectral irradiance as the source, the output of the monochromator was measured as a function of wavelength. The monochromator measurements were repeated with the standard of spectral irradiance replaced by the star simulator as the source. The spectral output of the star simulator was then calculated by use of the following formula:

$$\Phi_{SS}(\lambda) = \frac{\Phi_S(\lambda)\, V_{SS}(\lambda)}{V_S(\lambda)}$$

where

$\Phi_S(\lambda)$ standard of spectral irradiance as a function of wavelength

$\Phi_{SS}(\lambda)$ star-simulator irradiance as a function of wavelength

$V_S(\lambda)$ monochromator output with standard of spectral irradiance as source

$V_{SS}(\lambda)$ monochromator output with star simulator as source

Three spectral filters were used to match three selected star spectral classes. The selected classes were A0, G0, and M0, which were approximated by blackbody temperatures of 11 000°, 6000°, and 3100° K, respectively. The relative spectral characteristics of the simulated A0, G0, and M0 stars and their ideal blackbody curves are shown in figures 13, 14, and 15, respectively. A study was performed to estimate the response of the star mapper to the simulated stars and to the ideal blackbodies of exact temperatures. The results of this study showed that the spectral errors caused the output of the star mapper to be slightly less when viewing the star simulator than when viewing true blackbodies of the same visual effective irradiance. The differences in star-mapper output varied between 3 and 10 percent, depending on the star spectral class.

The absolute levels of the star-simulator spectral output were adjusted by use of neutral-density filters. The transmission values of the neutral-density filters were selected to control the effective visible irradiance of the star simulator when used with the test collimator. Corrections were made to the data to compensate for irregularities in the flatness of the spectral characteristics of the neutral-density filters. Tests were performed to determine the attenuation factors for each star class necessary to achieve an irradiance value of 3.1×10^{-13} watt/cm^2 for a star with a visual magnitude of 0. These tests were performed by using a standard photocell and filter combination with a spectral response equivalent to the human eye.

Star-mapper photometric calibration.- The test setup for the star-mapper photometric calibration was identical to that used for the field-of-view mapping accuracy (fig. 10). During the calibration test, the rotary table was held fixed in a position to obtain maximum output from the star mapper. The star mapper was then exposed to each of the three star spectral classes (A0, G0, and M0). For the A0 star with visual magnitude of 0, the system gain was adjusted until the star-mapper output signal reached a value of 4 volts. For each spectral class, the irradiance was varied from an equivalent star with $m_V = 0$ to a star with $m_V = +3$ in half-magnitude steps. Typical star-mapper outputs for four different visual magnitude stars of the A0 class are shown in figure 16. The signal-to-noise ratio (exclusive of background noise) was found to be approximately 13:1 for the stars with a visual magnitude of 0 of the A0 class. A summary of the calibration of the star mapper is shown in figure 17. An error analysis of this calibration method was performed, and results indicated that a variation of ±25 percent could be expected for in-flight irradiance measurements.

Sun-Shield Attenuation

The effectiveness of the sun-shield attenuation was evaluated for off-axis light sources. The first attempt to measure sun-shield attenuation utilized the same collimator used in the field-of-view mapping-accuracy test, with a chopped carbon arc as the simulated sun source. In an effort to reduce the effect of atmospheric scattering, the collimator and star mapper were sealed off from the room and purged with dry nitrogen. A dust precipitator was operated in the collimator system for 24 hours prior to testing. This test setup was abandoned when it was determined that attenuation factors less than 10^{-9} could not be accurately determined because of Rayleigh scattering.

In order to reduce the effects of Rayleigh scattering, the star mapper was placed in a 12-meter vacuum sphere where the ambient atmosphere was reduced to 10^{-5} torr. The walls of the chamber were draped with black floc and the field of view of the star mapper was protected from stray light by a black Carrara glass screen. A chopped carbon arc used as a source was located outside the vacuum sphere and an adjustable mirror was used to reflect the source at the required angles into the sun shield used in the star mapper. Figure 18 shows this test setup in which the source was chopped at a frequency within the bandwidth of star-mapper electronics and in which neutral-density filters were placed in front of the source to control the level of irradiance. The optical axis of the star mapper was rotated to an angle of 70° relative to the collimated beam and the neutral-density filters were adjusted until the star-mapper output was approximately 1 volt at this angle. A standard photocell was used to measure the level of irradiance at the star-mapper aperture, and the unattenuated response of the star mapper to this irradiance was calculated by using the calibration data. The sun-shield attenuation at the 70° off-axis angle was determined by the ratio of the measured output to computed unattenuated output. Changes in attenuation levels for other off-axis angles were determined by rotating the star mapper to a given angle and relating the new output to the output signal at the 70° case. These measurements were repeated for all four sides of the sun shield. A summary of the measured sun-shield attenuation data is shown in figure 19. As indicated in this figure, the sun shield did not meet the attenuation requirement of 10^{-12} at an angle of 25° off the optical axis.

A detailed examination of the sun-shield design indicated two possible reasons for failure to meet the attenuation requirement. First, since the painted magnesium baffles had edge radii on the order of 0.0076 centimeter, they were not sufficiently sharp. These edge surfaces permitted a single diffuse reflection to place solar energy on the first optical element. Second, large portions of the diffuse-reflecting inner surfaces of the baffles, receiving energy from the sunlit outer surfaces of adjacent baffles, directly illuminated the first optical element. Since the Scanner launch could be changed to a dark-of-night firing without compromising the experiment objectives, no attempt at a redesign was undertaken.

TRANSIT-TIME DETECTION

The data processing required to detect and identify the stars sighted by the instrument is briefly described. A detailed discussion of the data processing may be found in reference 2.

As previously discussed, a single-pulse sequence for a particular star transit consisted of an 8-bit code pattern. The code pattern produced by the reticle slit design was 1-1-0-1-0-0-0-1. Since the reticle is opaque, except for its transparent slits, the next bit in time would be a 0. This feature was used to add another 0 bit to the code group since a return to zero situation was desirable in the decoding operation. In order to improve on the time resolution of a detected-star transit, each bit of the code sequence was subdivided into four elements. With these changes a single star transit generated a code sequence of 36 bits.

A simplified diagram of the decoder is shown in figure 20. As indicated in this figure the raw star-mapper signals, range time, and two reference frequencies of 1 kilohertz and 100 kilohertz were tape recorded. The 100-kilohertz signal was used as a 10-microsecond vernier during 1-millisecond intervals. The raw star-mapper signals were converted to a two-level digital pulse train by use of an adjustable threshold. This 36-bit two-level coded-pulse sequence was compared in a correlator with a reference pulse sequence consisting of an equal number of bits. Detection threshold was set for two conditions of logic. Detection of a star transit across a sequence of transparent slits was acknowledged provided that comparison of the reference code sequence with a given sequence of 9 basic bits produced agreement of any two ones and all five zeros or three ones and four zeros. Acknowledgment of transit detection was in the form of a gating signal which enabled digital recording of range time of detection, threshold setting, and peak amplitude of the first pulse in a signal-pulse sequence. The peak-amplitude detector was reset to zero after each code-sequence recognition. The variable threshold and the tape recording feature permitted manual selection of a limited number of stars per vehicle revolution. This capability reduced the number of possible ambiguities in the subsequent star identification program. Detection times were set for the trailing edge of each 36-bit code sequence. Detection-time resolution was limited by the time duration of one element of the 36-bit code sequence and range-time uncertainties. The time duration of each bit of the 36-bit code sequence was controlled by a variable-clock pulse generator which was adjusted for the best estimate of vehicle spin rate and the angular resolution of the smallest transparent slit of the reticle. The spin-rate estimate was readjusted as attitude-determination results became available (ref. 2).

The results of the transit-time-detection processing were stored in a digital listing of apparent-star transit times and amplitudes of each apparent-star signal. This listing was hand sorted to pair the transit times for each apparent-star signal. This hand

sorting was accomplished by pairing of transit-time differences between apparent-star signals with the aid of the signal amplitude measurements. All transit-time differences that exceeded the constraints established by the geometry of the reticle slit configuration and estimated vehicle spin rate were rejected as false star indications. This modified listing of star transit times was then used in the routine of star identification which is discussed in detail in reference 2.

POST-FLIGHT EVALUATION OF STAR-MAPPER OPERATION

The star mapper was flown successfully on two Project Scanner flights, the first flight on August 16, 1966, and the second flight on December 10, 1966. A discussion of star-mapper data processing and attitude-determination results are given in reference 2. Figure 21 shows a typical scan of the Scanner flight 1 star-mapper field of view through the celestial sphere. This scan was reconstructed by use of the attitude-determination results and the flagged stars indicated in the figure are those identified and used for attitude determination. A check of the star-mapper calibration was attempted by using two randomly selected identified stars. Photographs of the coded star signals for the selected stars Alkaid and Alphecca are shown in figures 22 and 23, respectively. Each figure shows photographs of these star signals generated by the vertical group of slits for three different sighting times to demonstrate the severe noise problem introduced by background and signal-generated noise. In all photographs, the coded pattern is clearly evident and indicates the advantages of coded reticles for star-signal detection purposes. Alkaid and Alphecca are +1.91 visual magnitude B3 and +2.31 visual magnitude A0 stars with predicted star-mapper signal levels of 0.90 and 0.60 volt, respectively. Averaging ten sightings of each star resulted in output signal levels of 1.65 volts for Alkaid and 0.85 volt for Alphecca. Several other stars were examined in a similar manner and results indicated that the star mapper had a sensitivity which was 1.5 to 1.75 times greater than that expected from the preflight calibration results. A check of the star-mapper calibration over its dynamic range was not possible since none of the stars identified during the first flight were predicted to produce outputs greater than 1 volt.

The average background noise was expected to be approximately equivalent to the signal produced by a +4 visual magnitude A0 star. No attempt was made to verify this expected background noise level because of the existence of numerous low-intensity stars that were identifiable as star signals although not identified for attitude-determination purposes. However, a rough approximation of the peak-to-peak noise level due to background noise may be determined from an examination of figures 22 and 23. In each figure, the average peak-to-peak background noise level is approximately 0.3 volt or a root-mean-square (rms) value of 0.11 volt. By using the signal and noise definitions of reference 3, the ratio of average signal level to rms background level was predicted to be

approximately 9.25:1 for an assumed +2.3 visual magnitude A0 star. The average in-flight signal of 0.85 volt obtained for Alphecca and the average rms background level of 0.11 volt indicate a signal-to-noise ratio of 8:1. These values agree favorably and indicate validity of the assumed signal and noise models used in the design of the star mapper.

Figure 24 is a sample record of the output of the star mapper and presents a basic picture of the in-flight performance. The record shows the signals generated by the transits of two different stars across the vertical and slanted groups of slits. The code groups are degraded somewhat due to the frequency response of the oscillograph. One of the stars identified on this trace is a +2.92 visual magnitude A3 star. A listing of all stars identified during Project Scanner flight 1 is given in table 3 (see also ref. 2). These stars are listed according to their Boss catalog number, star name, Bayer name, constellation, visual magnitude, and spectral class. The lowest intensity visual magnitude star identified from the star-mapper data of the first flight was a B8 star with a visual magnitude of +3.30; the lowest intensity star, relative to the instrument spectral response, identified from data of the first flight was an M3 star with a visual magnitude of +3.19. The results of Project Scanner flight 2 were very similar and a listing of all stars which were detected and identified during the second flight are shown in table 4. It can therefore be seen that the design goal of detecting and identifying stars in a +3 visual magnitude A0 spectral class was met.

CONCLUDING REMARKS

The successful application of the star mapper to solve the attitude determination problem of Project Scanner provided a flight demonstration of a highly accurate method of determining the celestial attitude of a spinning spacecraft. For the star mapper flown on Project Scanner, it was possible to correlate flight measurements to laboratory calibration. The results demonstrated that the goal of detecting and identifying stars in a +3 visual magnitude A0 spectral class was achieved, the photometric calibration was verified within a factor of 2, the system fidelity provided star transit-time measurements within the required resolution and accuracy, and the theoretical predictions of signal-to-noise ratios were in close agreement with flight measurements. A significant problem that was not resolved was the design and construction of a sun shield having the required attenuation of stray sunlight to allow daylight operation.

Langley Research Center,
National Aeronautics and Space Administration,
Langley Station, Hampton, Va., May 24, 1968,
715-02-00-01-23.

REFERENCES

1. McKee, Thomas B.; Whitman, Ruth I.; and Davis, Richard E.: Infrared Horizon Profiles for Summer Conditions From Project Scanner. NASA TN D-4741, 1968.

2. Walsh, T. M.; Keating, Jean C.; and Hinton, Dwayne E.: Attitude Determination of Spin-Stabilized Project Scanner Spacecraft. NASA TN D-4740, 1968.

3. Walsh, T. M.; and Kenimer, Robert L.: Analysis of a Star-Field Mapping Technique for Use in Determining the Attitude of a Spin-Stabilized Spacecraft. NASA TN D-4637, 1968.

4. Chapman, R. M.; and Carpenter, R. O'B.: Effect of Night Sky Backgrounds on Optical Measurements. GCA Tech. Rep. 61-23-A, Geophys. Corp. Amer., May 22, 1961.

5. Kauth, Richard: Backgrounds. Handbook of Military Infrared Technology, William L. Wolfe, ed., Office Naval Res., Dep. Navy, 1965, pp. 95-173.

6. Roach, F. E.; and Megill, Lawrence R.: Integrated Starlight Over the Sky. Astrophys. J., vol. 133, no. 1, Jan. 1961, pp. 228-242.

TABLE 1.- PROJECT SCANNER SPACECRAFT

Vehicle: Modified Trailblazer II configuration – three stages
  First stage – Junior rocket motor with two Recruit assist rocket motors
  Second stage – Skat rocket motor
  Third stage – Altair I-A6 rocket motor

Payload mass: 254 kilograms (includes burned out Altair motor case)

Payload size: Nominally 61 centimeters in diameter and 366 centimeters long

Launch site: NASA Wallops Station

Nominal trajectory (radar and telemetry signals received until spacecraft impact):
  Apogee, 740-kilometer altitude
  Impact, 1111-kilometer range
  Spin rate, 270 deg/sec during data period

TABLE 2.- SCANNER STAR-MAPPER ENVIRONMENTAL QUALIFICATION TEST LEVELS

1. Linear acceleration for 30 seconds along –
   - +X-axis 50g
   - -X-axis 10g

2. Steady-state spin rate for 450 seconds about –
   - X-axis . . . . . 350 rpm

3. Angular deceleration from 400 to 0 rpm about –
   - X-axis . . . . . 200 rad/sec^2

4.

Frequency range	Vibration along –	
	X-axis	Y- and Z-axes
5 to 12 Hz	1.27 cm (double amplitude)	0.635 cm (double amplitude)
12 to 100 Hz	±4g	±2g
100 to 500 Hz	±10g	±5g
500 to 2000 Hz	±20g	±8g
475 to 675 Hz	±60g	±11g

5. Random vibration (20 to 2000 Hz) for 6 minutes along –
   - X-axis . . . . . 0.08g^2/Hz
   - Y- and Z-axes . . . . . 0.04g^2/Hz

6. Shock (15-millisecond duration) along –
   - X-axis 75g
   - Y- and Z-axes 30g

7. Temperature . . . . . 261^o to 327^o K (95% humidity at 327^o K)

TABLE 3.- IDENTIFIED STARS OF PROJECT SCANNER FLIGHT 1

Boss catalog number	Star name	Bayer name	Visual magnitude, m_V	Spectral class
* 3584	Acamar	θ Eridani	3.06	A2
6274	Cursa	β Eridani	2.92	A3
6668	Bellatrix	γ Orionis	1.70	B2
6847	Mintaka	δ Orionis	2.48	O9
8208	Tejat Posterior	μ Geminorum	3.19	M3
12407	Talitha	ι Ursae Majoris	3.12	A4
15145	Merak	β Ursae Majoris	2.44	A1
16268	Phekda	γ Ursae Majoris	2.54	A0
17518	Alioth	ϵ Ursae Majoris	1.68	A0
*18133	Mizar	ζ Ursae Majoris	2.17	A2
18643	Alkaid	η Ursae Majoris	1.91	B3
20947	Alphecca	α Corona Borealis	2.31	A0
22193	Kornephoros	β Herculis	2.81	G8
25180	Kaus Borealis	λ Sagittarii	2.94	K1
25661		φ Sagittarii	3.30	B8
25941	Nunki	σ Sagittarii	2.14	B3
*26161	Ascella	ζ Sagittarii	2.71	A4
30942	Alnair	α Gruis	2.16	B5

*Double star.

TABLE 4.- IDENTIFIED STARS OF PROJECT SCANNER FLIGHT 2

Boss catalog number	Star name	Bayer name	Visual magnitude, m_V	Spectral class
519	Ankaa	α Phoenicis	2.44	G5
9188	Adara	ϵ Canis Majoris	1.63	B1
9443	Wezen	δ Canis Majoris	1.98	G3
9886	Aludra	η Canis Majoris	2.43	B5
13926	Regulus	α Leonis	1.34	B7
*14177	Algieba	γ^1 Leonis	2.61	K0
18643	Alkaid	η Ursae Majoris	1.91	B3
25466	Vega	α Lyrae	.14	A1
30491	Deneb Algiedi	δ Capricorni	2.98	A5
32000	Fomalhaut	α Piscis Austrini	1.29	A2

*Double star.

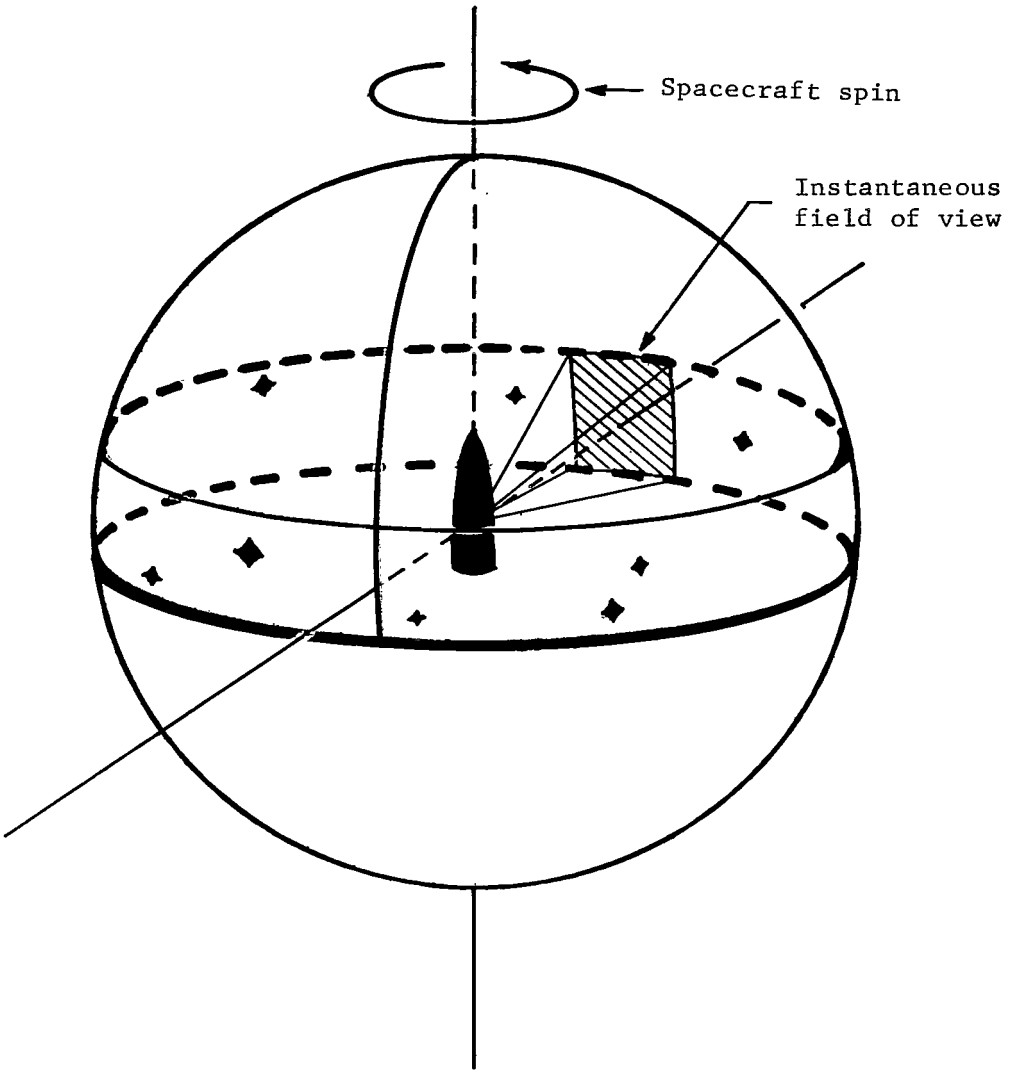

Figure 1.- Simplified representation of star mapping.

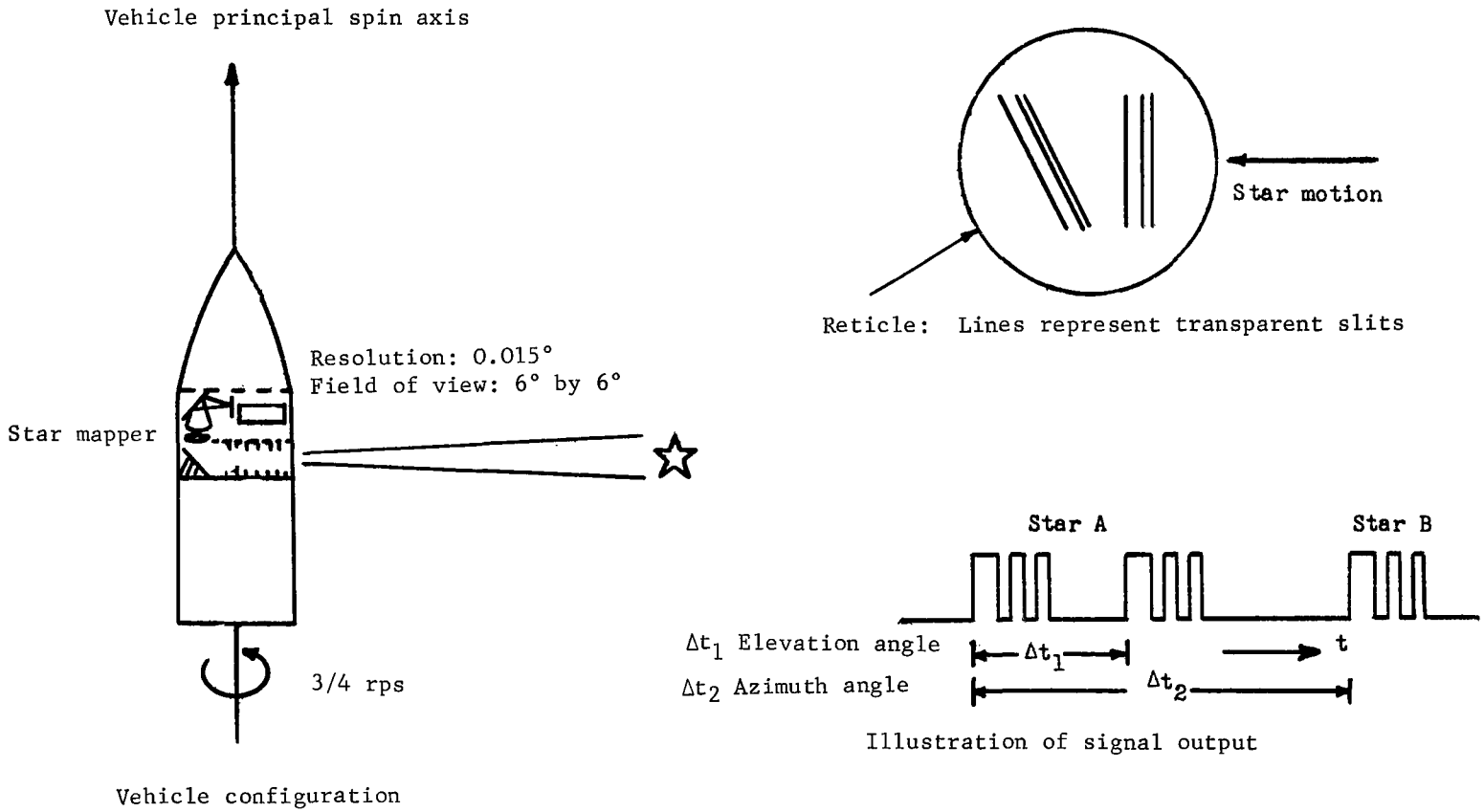

Figure 2.- Star-mapper concept.

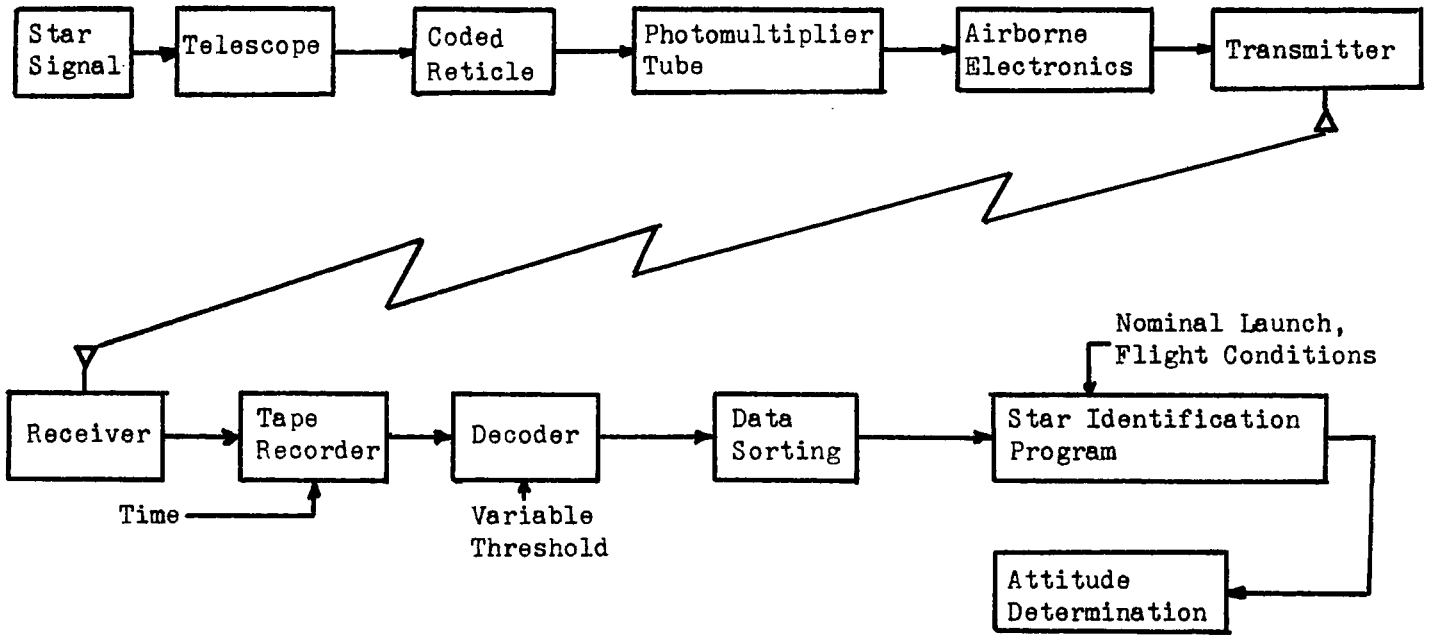

Figure 3.- Simplified signal flow diagram.

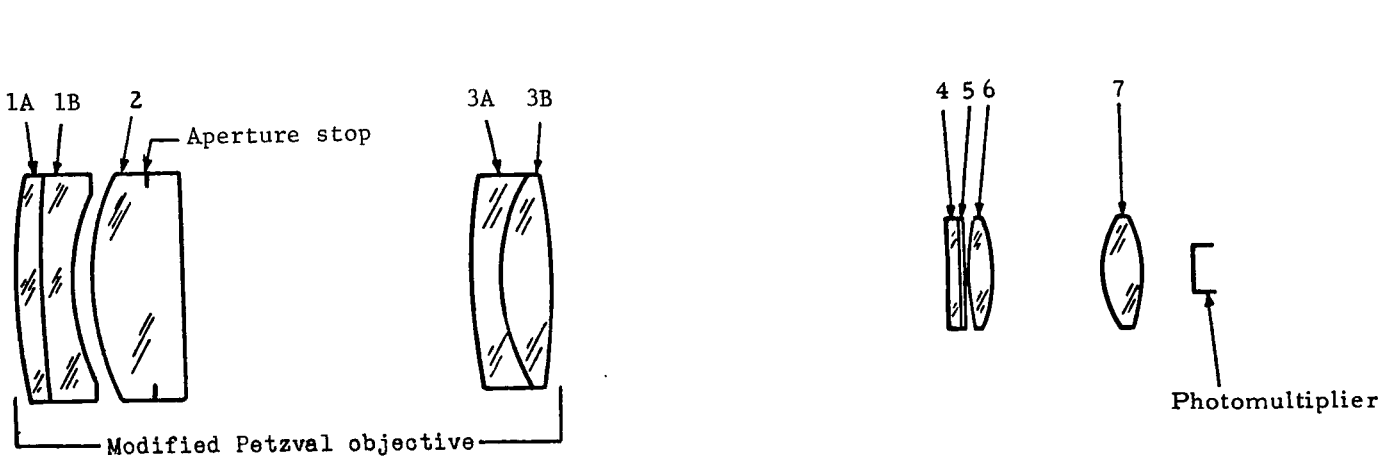

Effective focal length 38.100 centimeters
f/3.0

Note: Antireflection coating of magnesium fluoride on all exposed surfaces of optical elements.

Lens number	Function	Glass type	Clear aperture (centimeters)
1A	Objective	F-1	14.288
1B		KzFS-4	12.543
2		BK-7	12.289
3A		KzFS-4	13.493
3B		BK-7	13.493
4	Field flattener	BK-7	6.985
5	Reticle		
6	Field lens	BK-7	6.985
7	Field lens	BK-7	7.142

Figure 4.- Star-mapper optical layout.

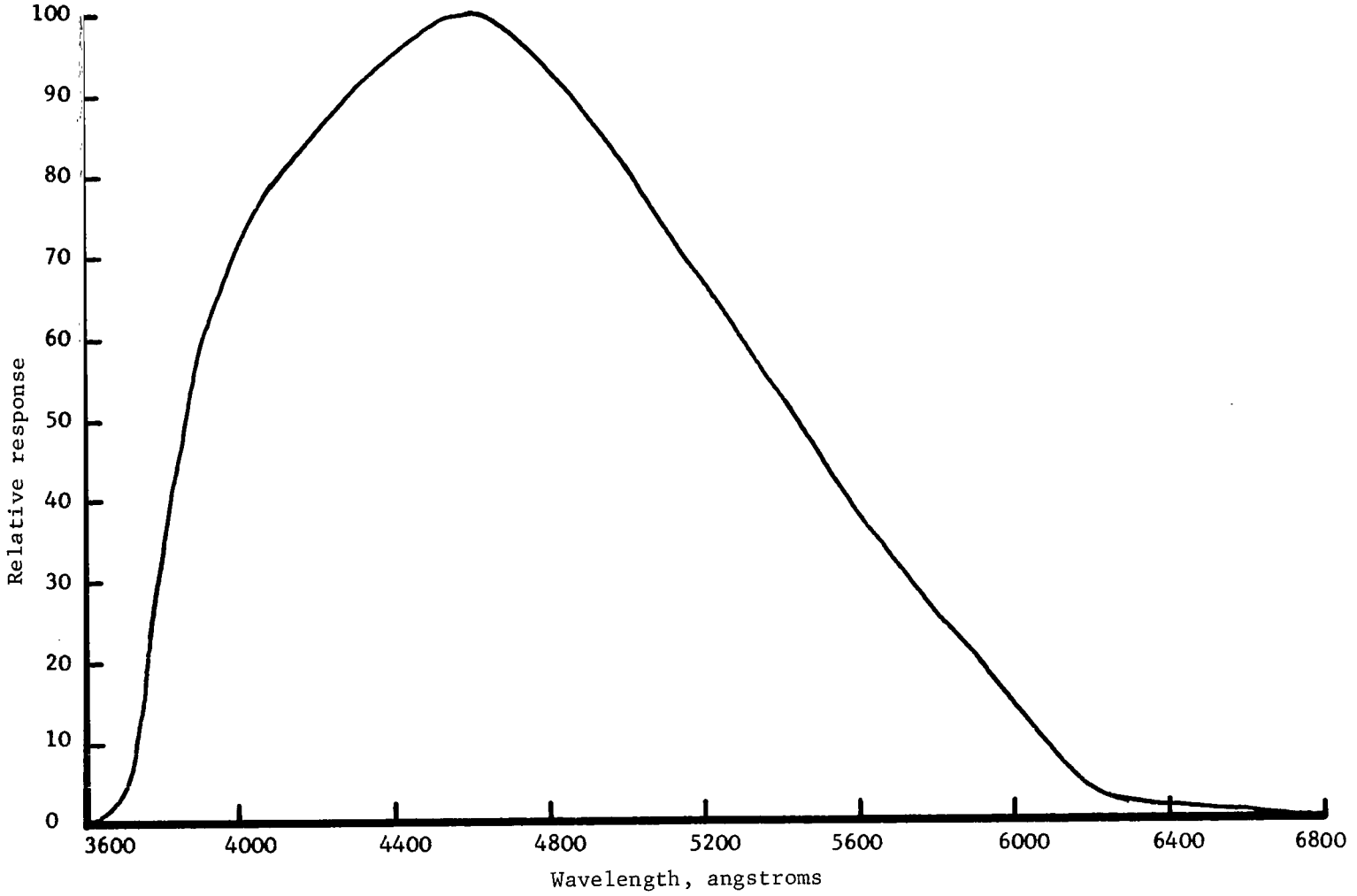

Figure 5.- Measured spectral response of flight 1 star mapper.

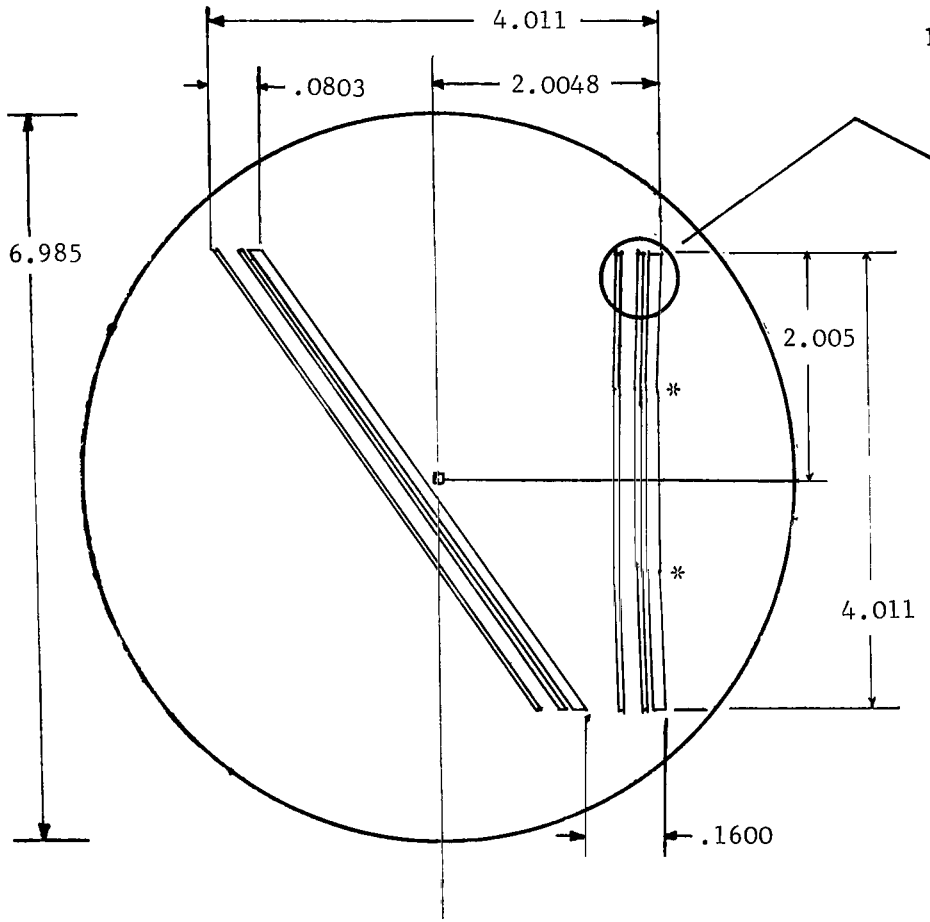

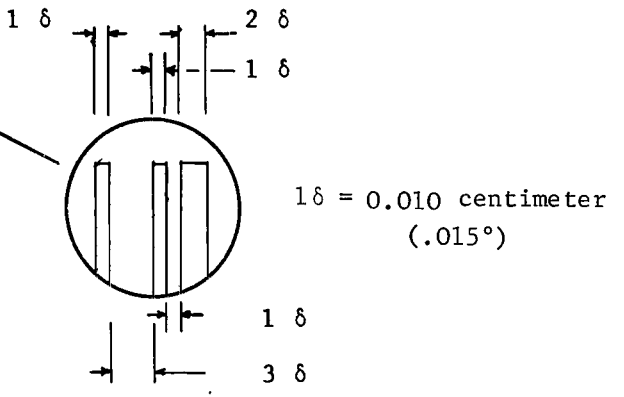

NOTES:

1. Transmissivity of clear area in slits = 95%
2. Transmissivity of opaque area less than 0.1%
3. Dimensions in centimeters
4. Slit widths are shown exaggerated for clarity.
5. * indicates break points for the three line segments required for distortion correction

Figure 6.- Reticle design.

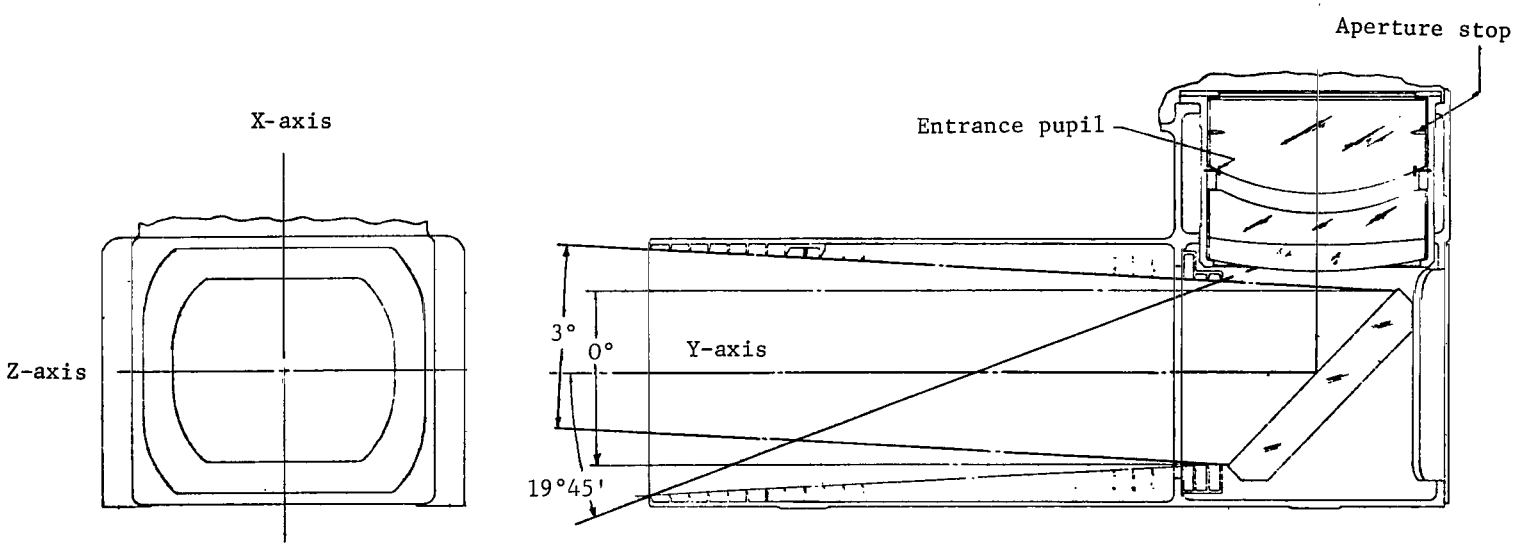

Figure 7.- Star-mapper baffle and obscuration layout.

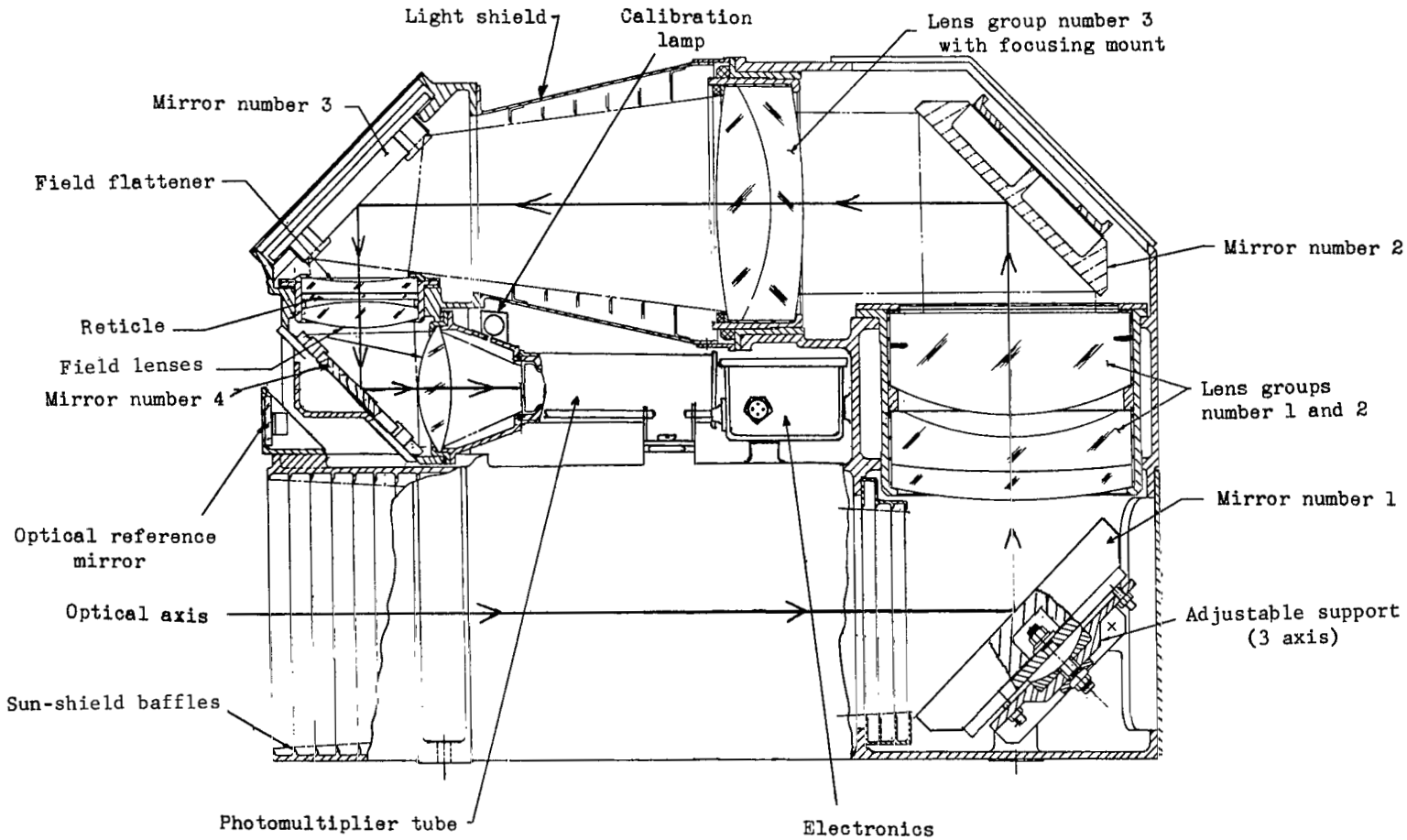

Figure 8.- Star-mapper assembly layout.

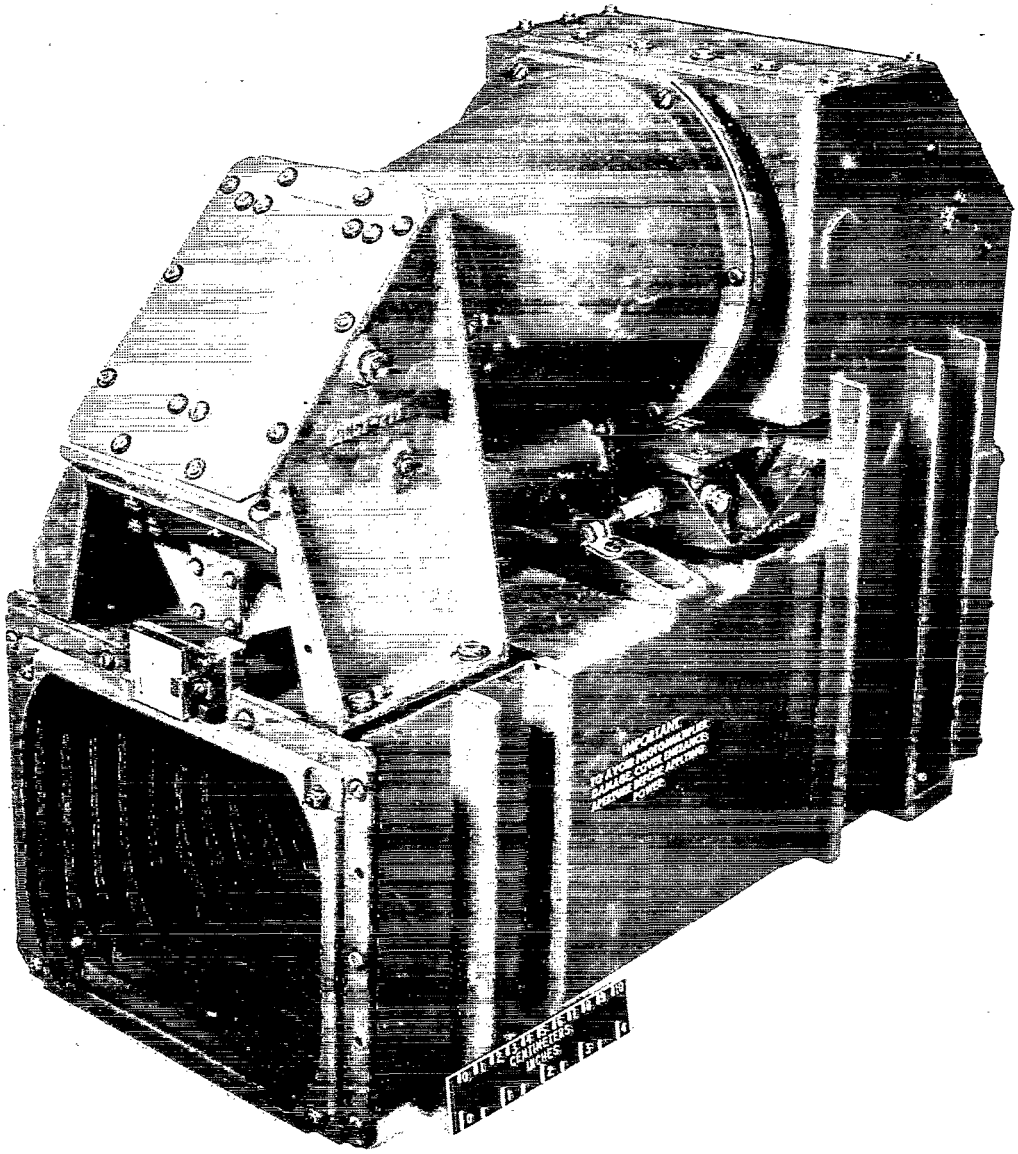

Figure 9.- Project Scanner star mapper. L-67-2286

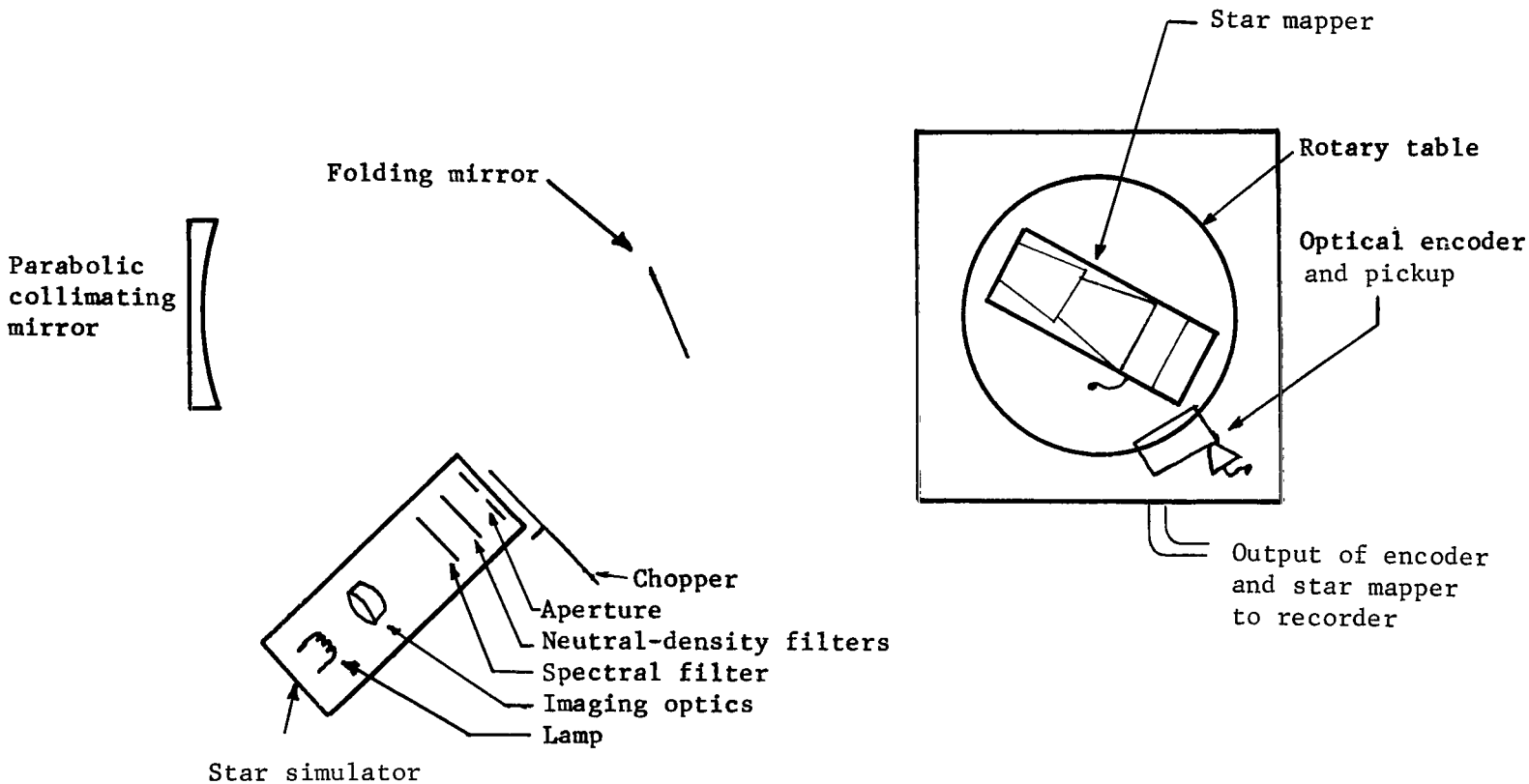

Figure 10.- Test setup for measuring field-of-view mapping accuracy.

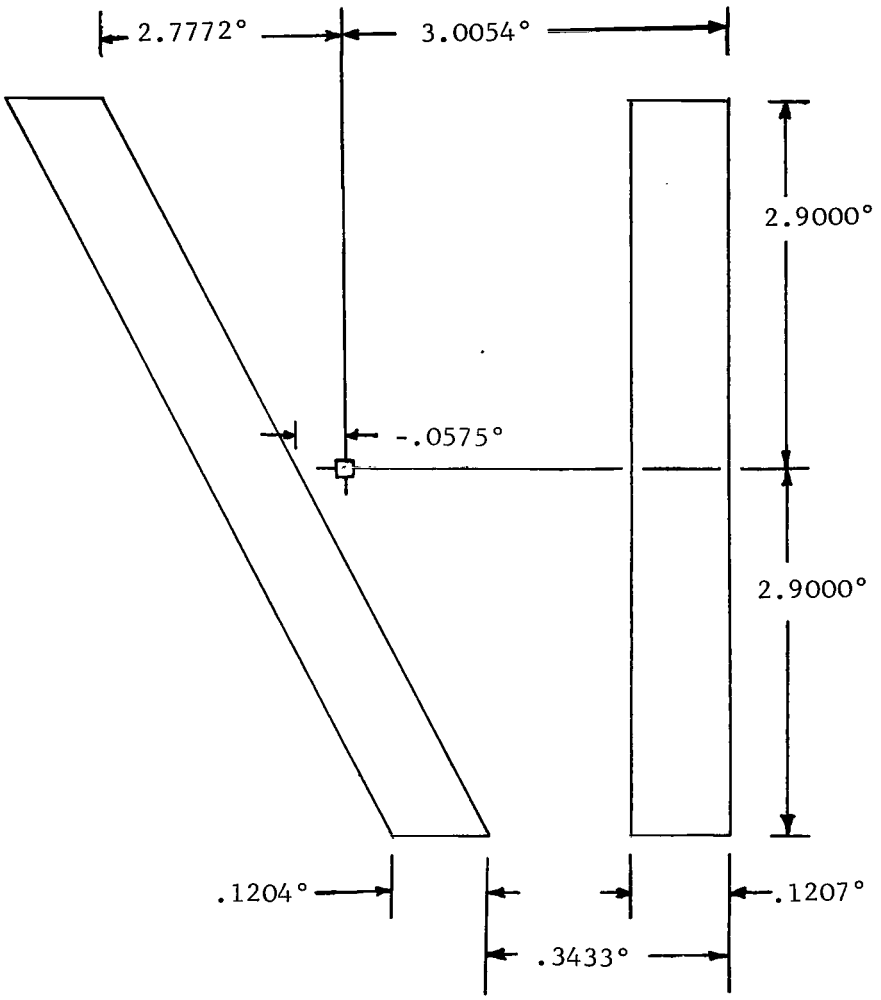

Figure 11.- Reconstruction reticle outline.

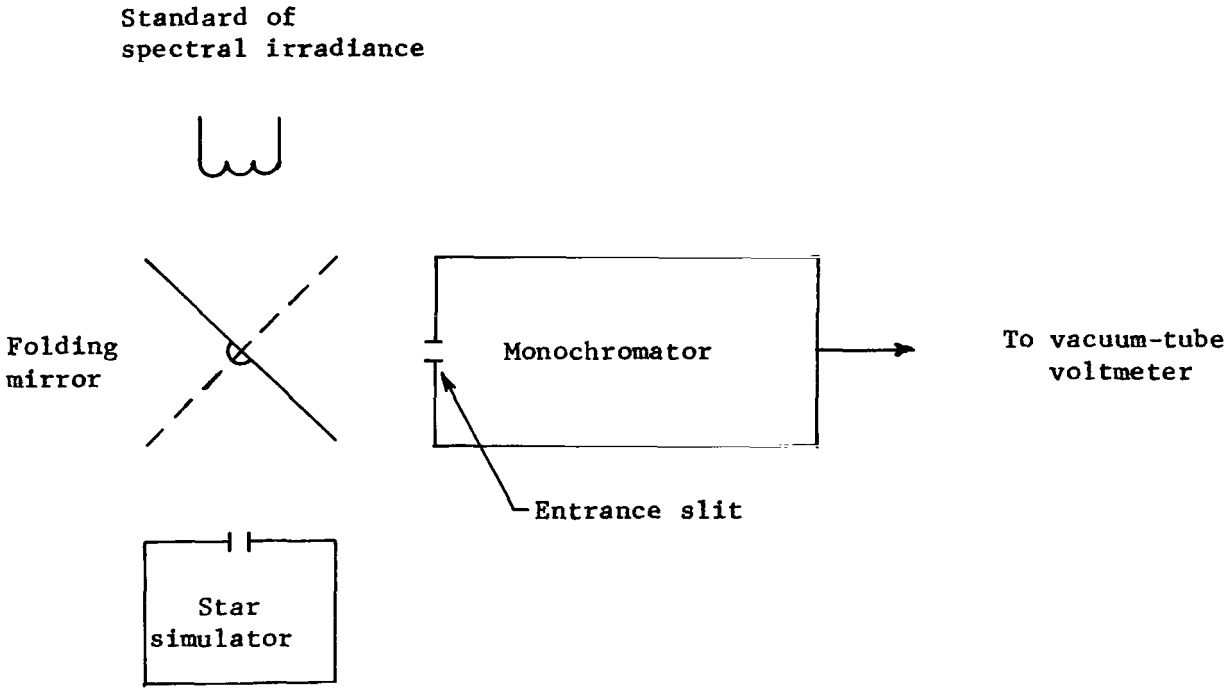

Figure 12.- Test setup used for star-simulator photometric calibration.

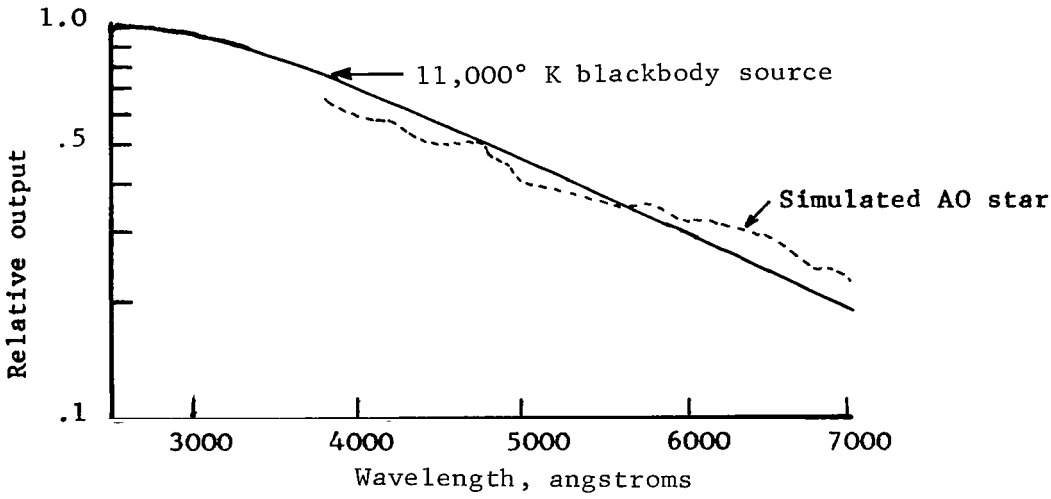

Figure 13.- Comparison of A0 star with 11 000° K blackbody source.

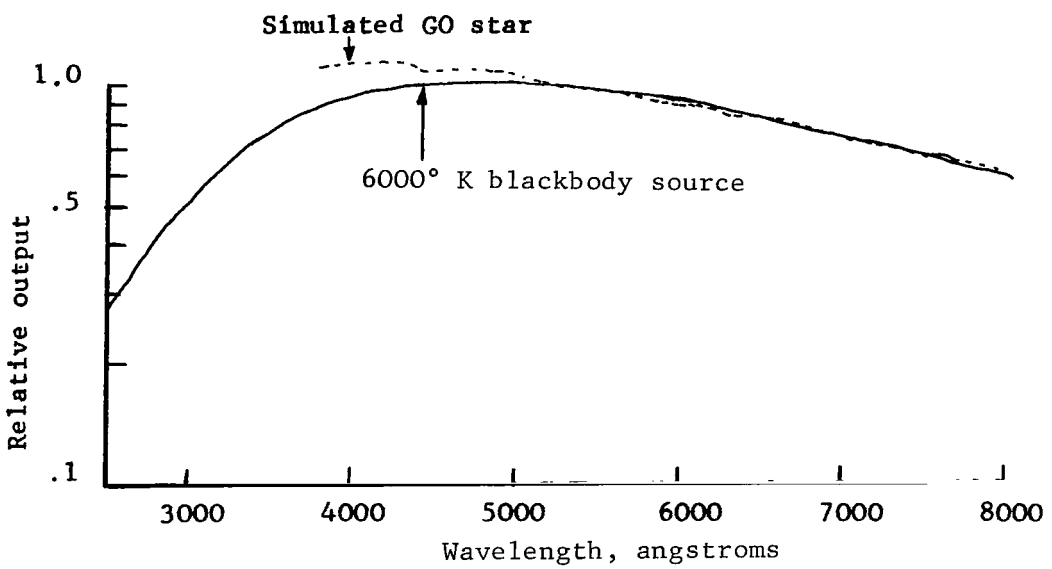

Figure 14.- Comparison of GO star with 6000° K blackbody source.

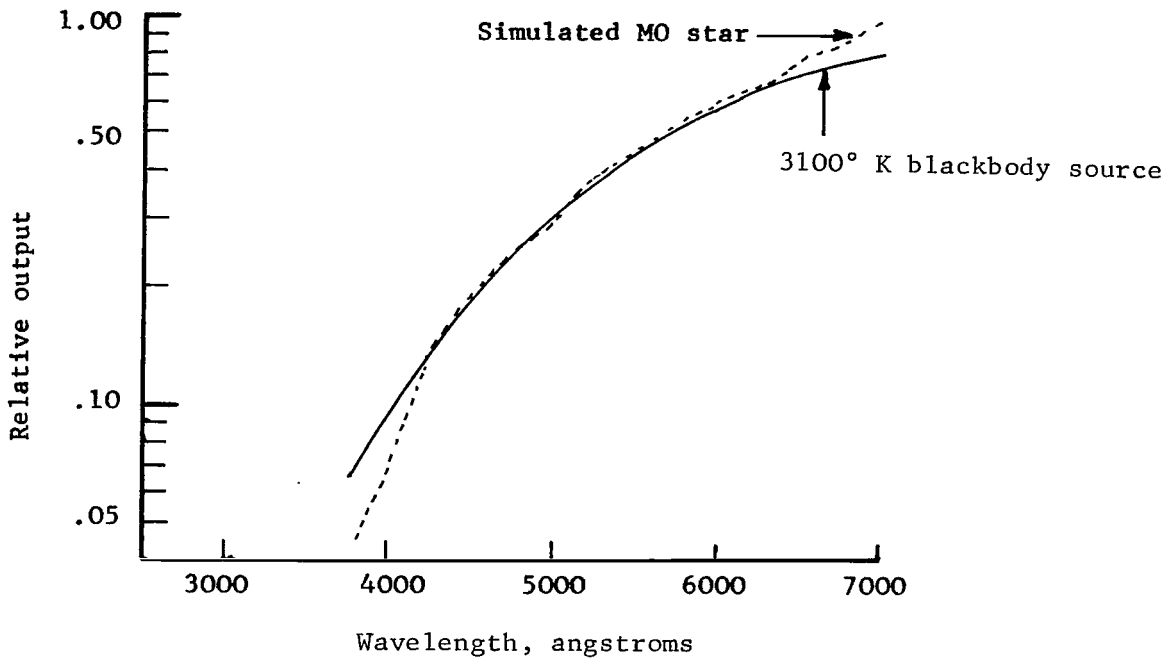

Figure 15.- Comparison of simulated MO star with 3100° K blackbody source.

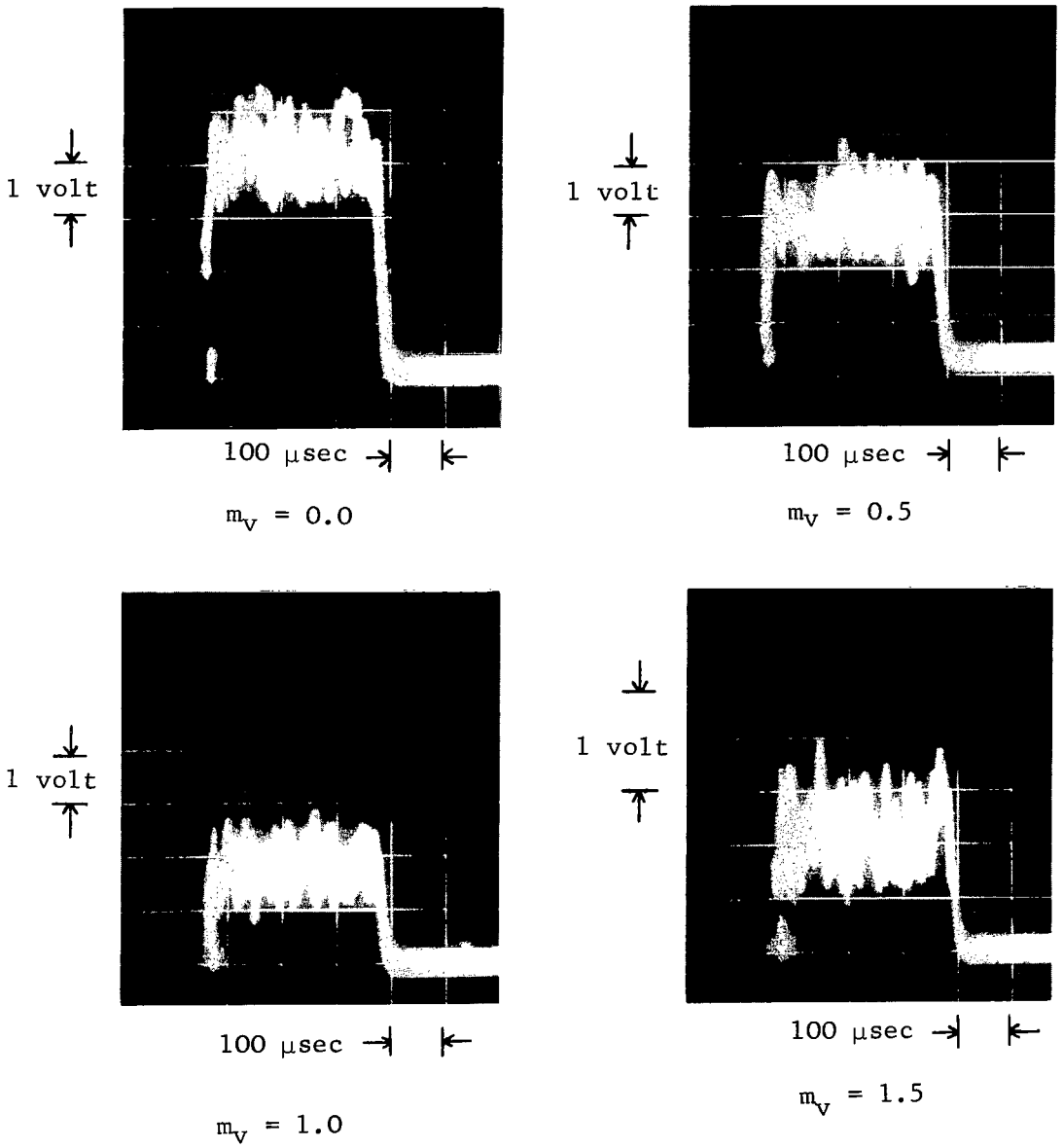

Figure 16.- Typical star-mapper outputs for simulated stars of the A0 spectral class.

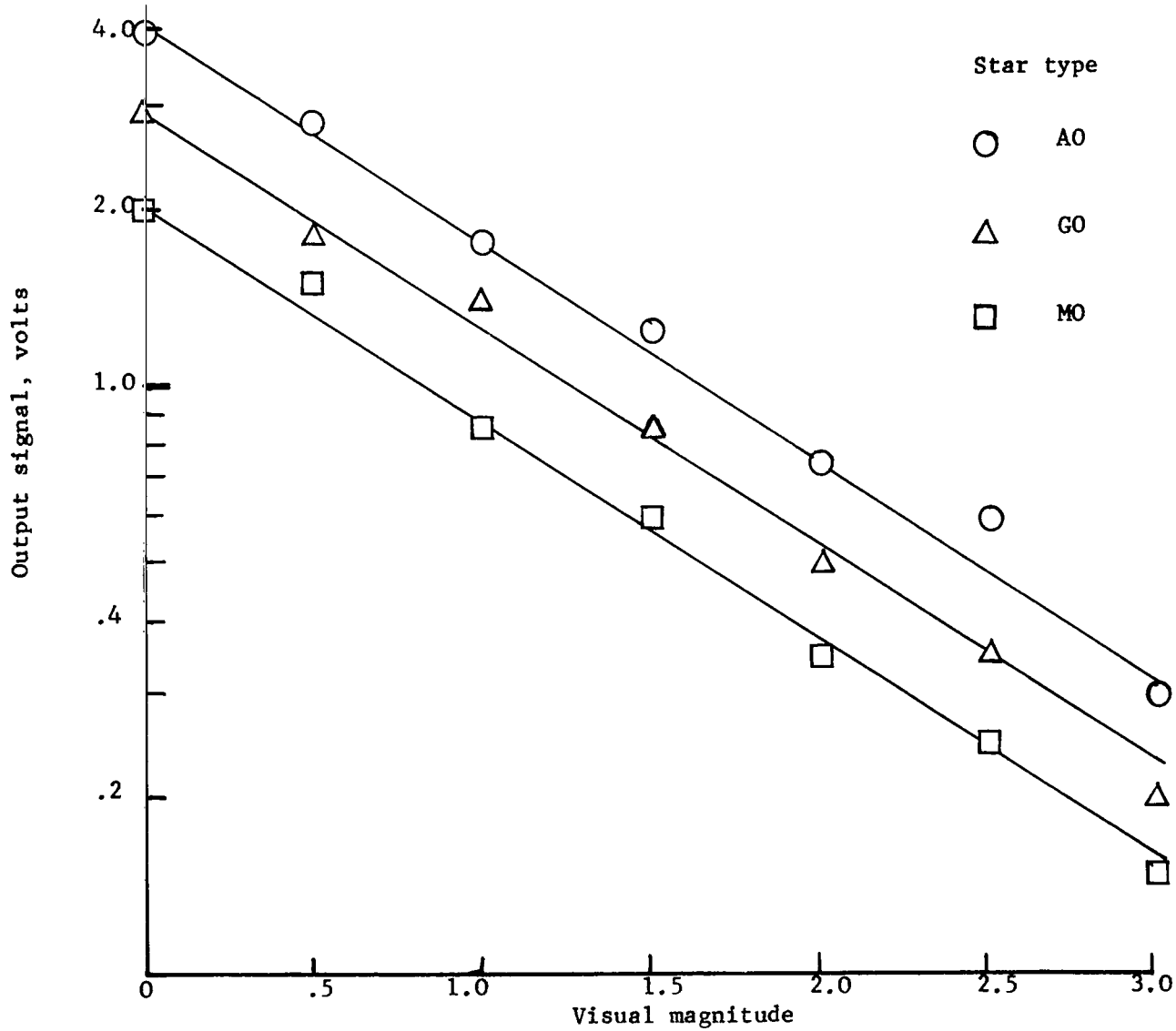

Figure 17.- Star-mapper calibration.

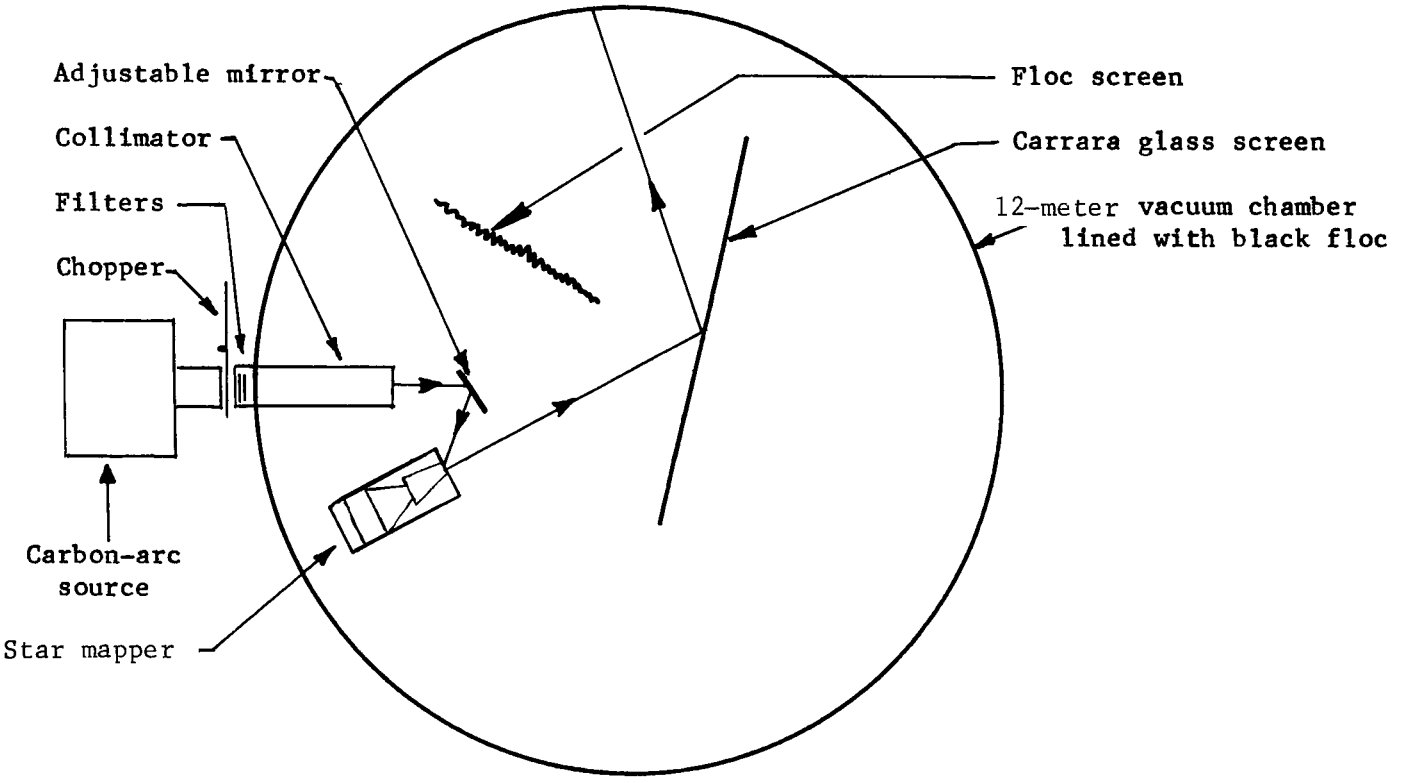

Figure 18.- Schematic setup of sun impingement test facility.

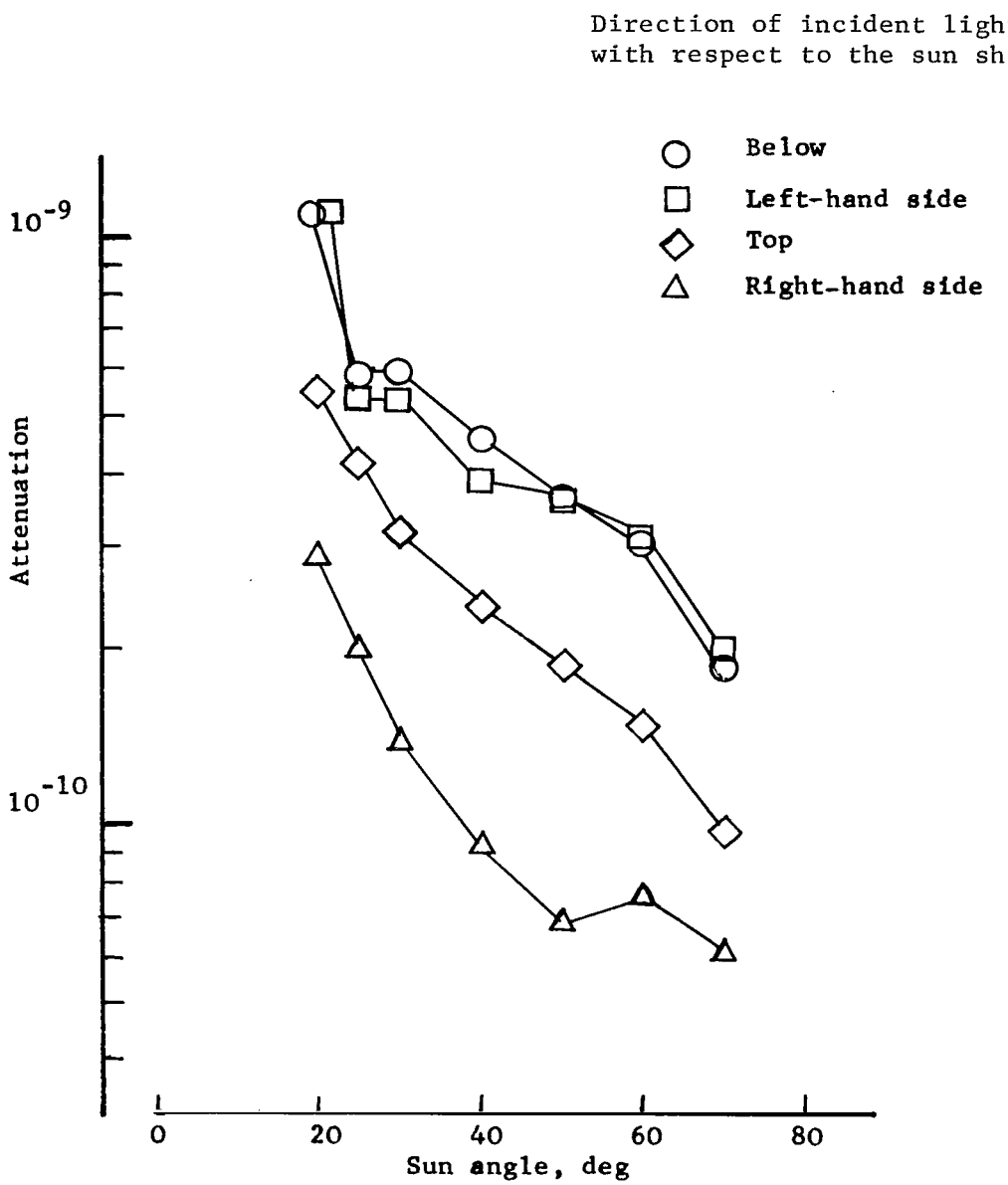

Figure 19.- Star-mapper sun-shield attenuation data.

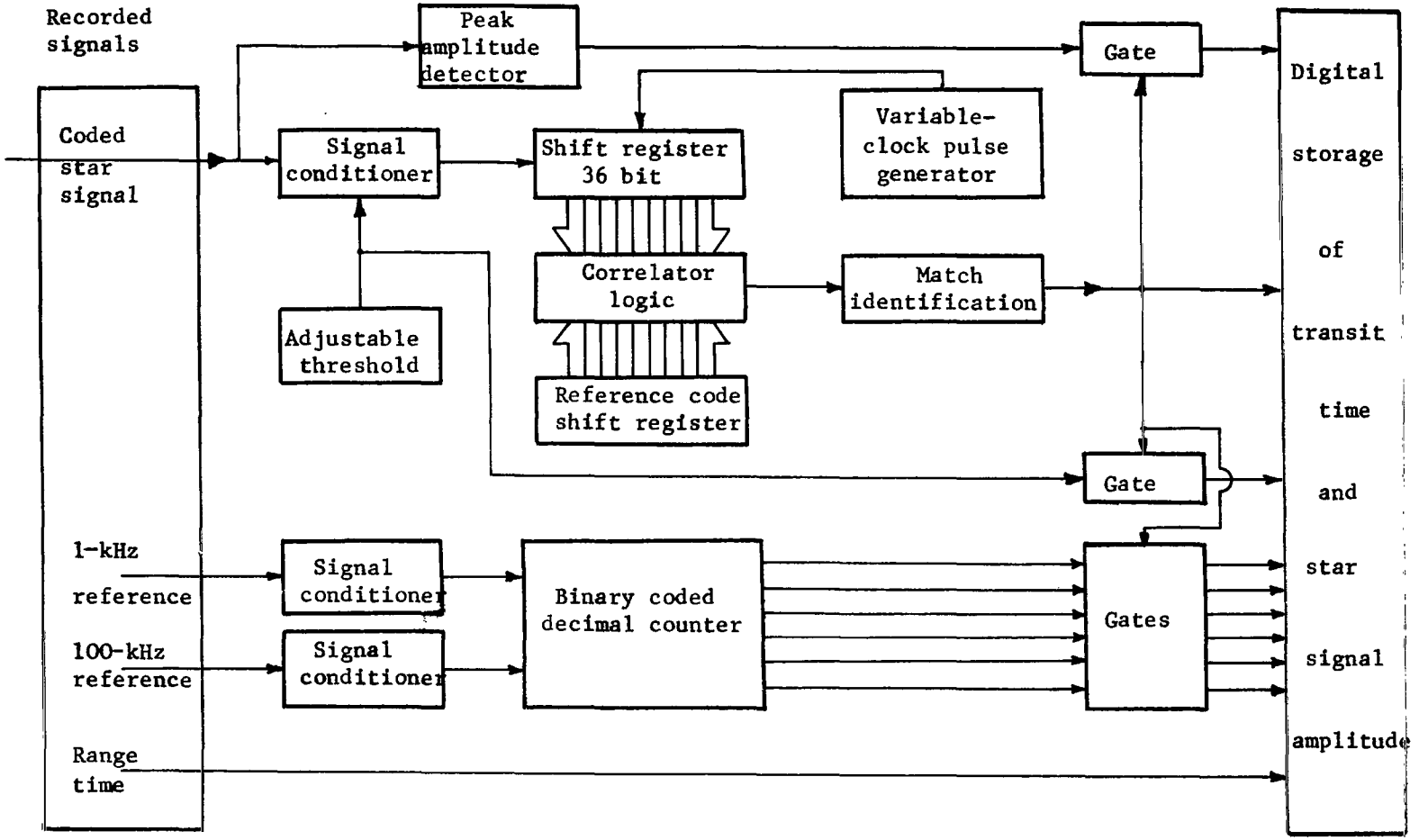

Figure 20.- Decoding of star-mapper signals.

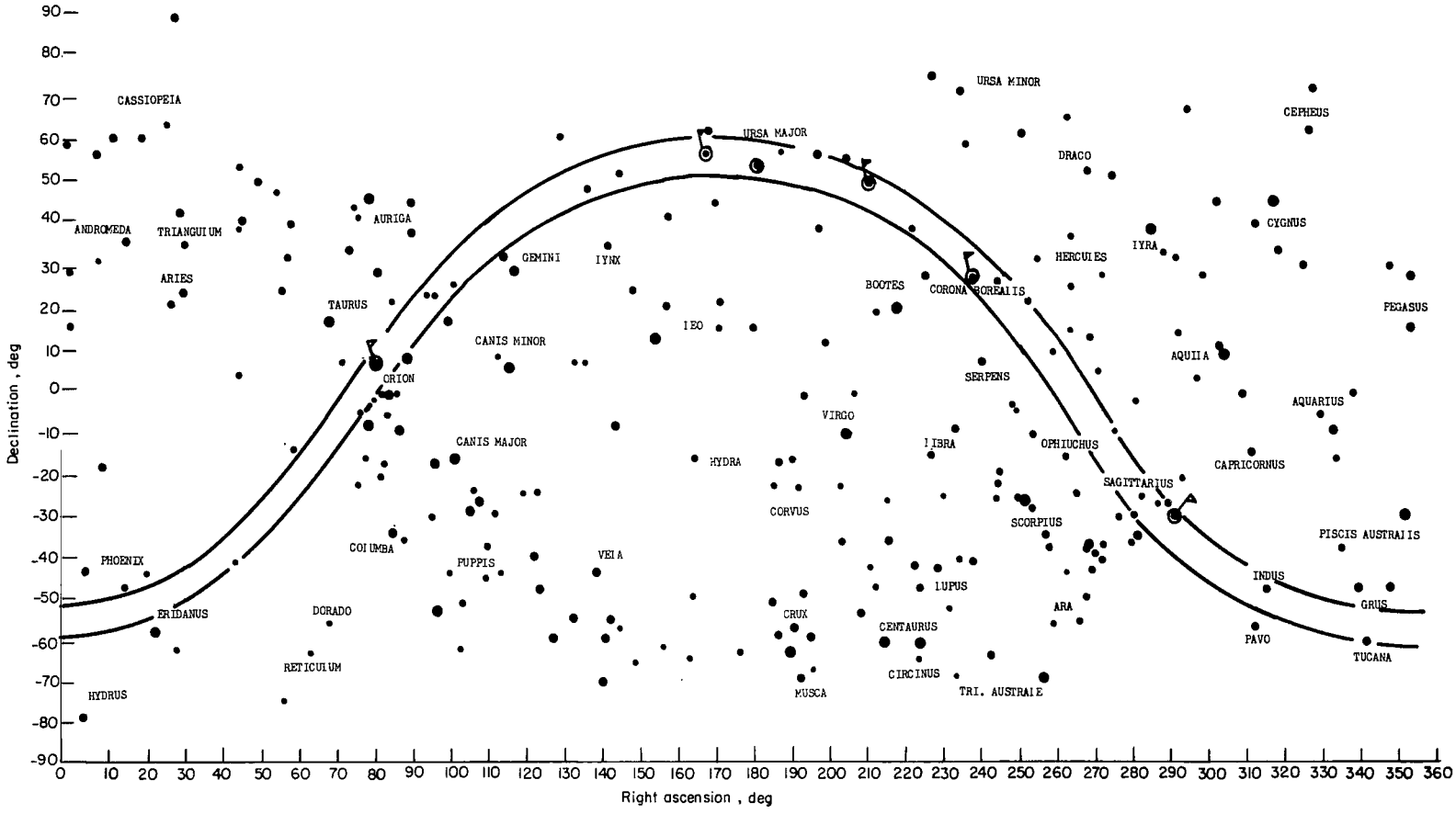

Figure 21.- Typical scan of star-mapper field of view. Project Scanner flight 1. (Flags indicate stars utilized in data reduction.)

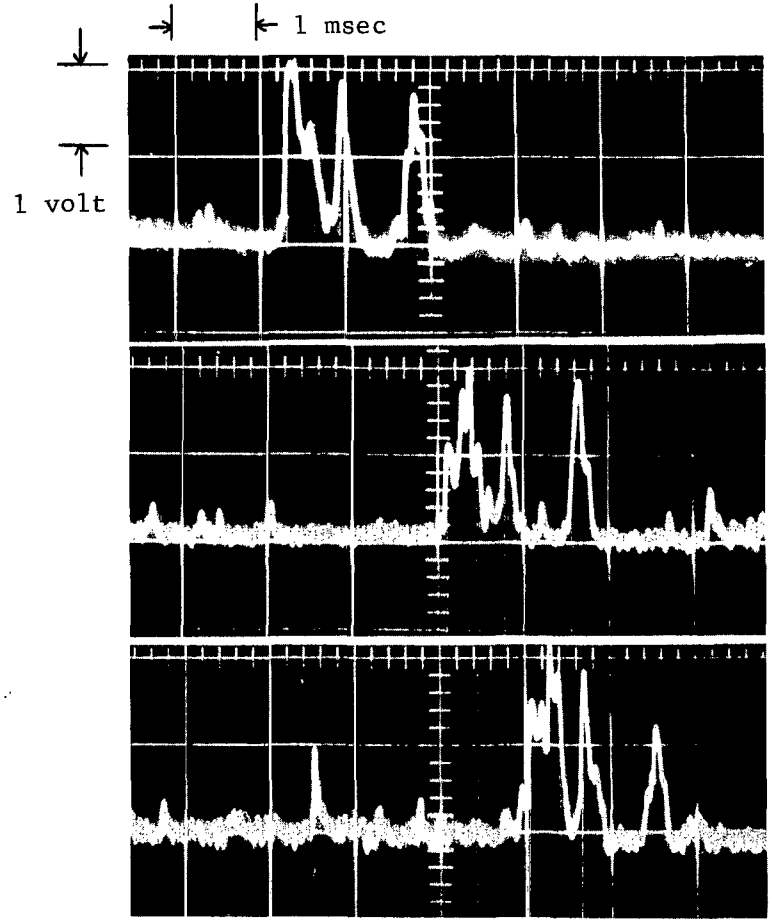

Figure 22.- Typical star signals from Alkaid.

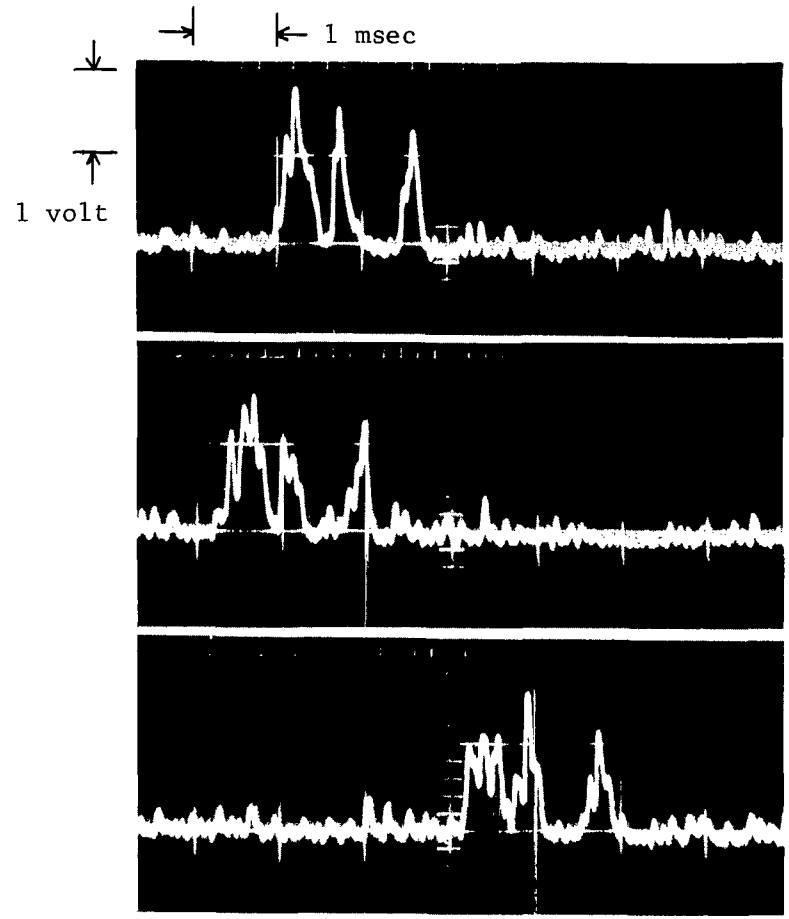

Figure 23.- Typical star signals from Alphecca.

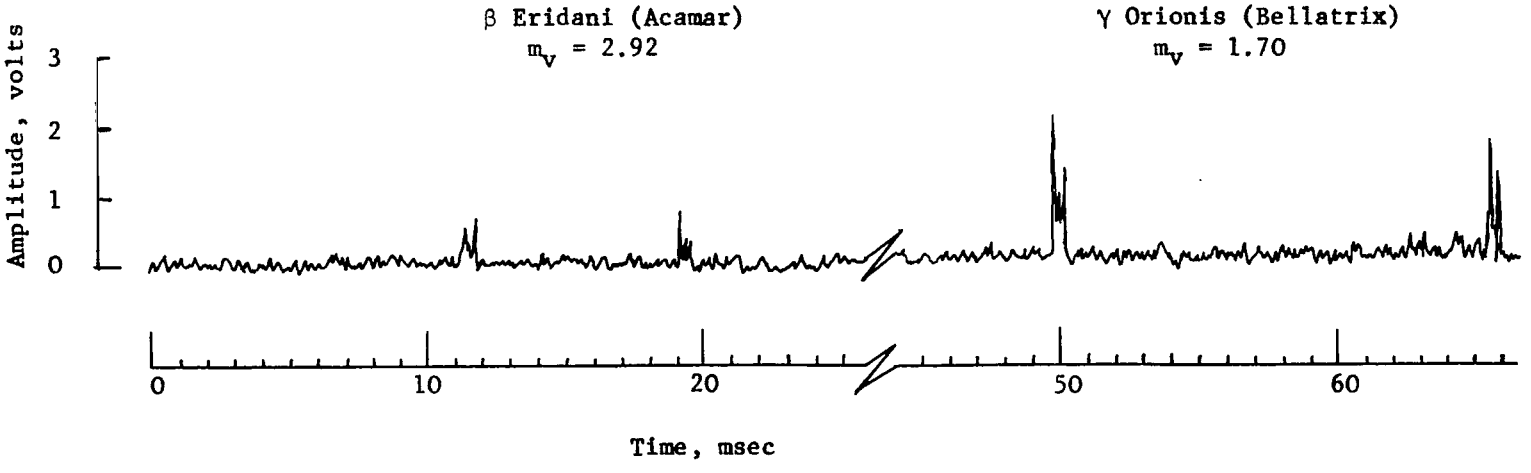

Figure 24.- Oscillograph record of output of star mapper.

NATIONAL AERONAUTICS AND SPACE ADMINISTRATION
WASHINGTON, D.C. 20546
OFFICIAL BUSINESS

FIRST CLASS MAIL

POSTAGE AND FEES PAID
NATIONAL AERONAUTICS AND
SPACE ADMINISTRATION

POSTMASTER: If Undeliverable (Section 158 Postal Manual) Do Not Return

"The aeronautical and space activities of the United States shall be conducted so as to contribute . . . to the expansion of human knowledge of phenomena in the atmosphere and space. The Administration shall provide for the widest practicable and appropriate dissemination of information concerning its activities and the results thereof."

—NATIONAL AERONAUTICS AND SPACE ACT OF 1958

NASA SCIENTIFIC AND TECHNICAL PUBLICATIONS

TECHNICAL REPORTS: Scientific and technical information considered important, complete, and a lasting contribution to existing knowledge.

TECHNICAL NOTES: Information less broad in scope but nevertheless of importance as a contribution to existing knowledge.

TECHNICAL MEMORANDUMS: Information receiving limited distribution because of preliminary data, security classification, or other reasons.

CONTRACTOR REPORTS: Scientific and technical information generated under a NASA contract or grant and considered an important contribution to existing knowledge.

TECHNICAL TRANSLATIONS: Information published in a foreign language considered to merit NASA distribution in English.

SPECIAL PUBLICATIONS: Information derived from or of value to NASA activities. Publications include conference proceedings, monographs, data compilations, handbooks, sourcebooks, and special bibliographies.

TECHNOLOGY UTILIZATION PUBLICATIONS: Information on technology used by NASA that may be of particular interest in commercial and other non-aerospace applications. Publications include Tech Briefs, Technology Utilization Reports and Notes, and Technology Surveys.

Details on the availability of these publications may be obtained from:

SCIENTIFIC AND TECHNICAL INFORMATION DIVISION

NATIONAL AERONAUTICS AND SPACE ADMINISTRATION

Washington, D.C. 20546